Norwegian University of Life Sciences
Faculty of Environmental Science & Technology
Dept. of Mathematical Science & Technology

Master Thesis 2015
30 credits

Cryospheric Mass Variations from GRACE

Kryosfæriske Massevariasjoner fra GRACE

Karoline Skår

Norwegian University of Life Sciences

Faculty of Environmental Science and Technology

Department of Mathematical Sciences and Technology (IMT)

Cryospheric mass variations from GRACE

Author:
Karoline Skår

Supervisors:
Dr.-Ing Christian Gerlach
Prof. Bjørn Ragnvald Pettersen

May 15, 2015

Norwegian University
of Life Sciences

Abstract

The Earth's gravity field is constantly changing due to mass redistribution from ice melting in the cryosphere and geophysical processes. With use of data from dedicated gravity satellite missions variations in the Earth's gravity field over a time series can be determined.

This thesis tries to give an explanation on how the Earth's gravity field changes on a global scale and regionally with the use of data from the GRACE-mission over a time period. With comparison between three different GRACE-solutions and the use of SLR-observations, the mass changes over Greenland has been estimated. In addition, a further look into the lower degree spherical harmonics has been studied, to explain and give a conclusion of how the lower degree spherical harmonics from GRACE are affecting the calculations of the gravity field.

GRACE-data has its uncertainties in the lower degree spherical harmonics. The C_{20}-coefficients from GRACE has large variances and therefore needs to be replaced by SLR-values when looking at global variations. Trend calculations shows how post glacial rebound(GIA) influence Canada and Fennoscandia, and ice melting over Greenland, Alaska and Antarctica.

The investigation of lower degree spherical harmonic coefficients shows that it is not significant how the C_{20}-coefficients are processed when estimating mass changes over the area of Greenland.

Due to restricted spatial resolution of the gravity field models and spatial averaging, it is hard to get a real estimate of the mass changes over a specific area. This is called the leakage effect and has been studied over the area of Greenland. The leakage effect has been estimated and restored, and mass change over Greenland has been estimated to be between -1832.76 km^3 and -2087.72 km^3, depending on the model used.

Sammendrag

Jordas tyngdefelt er i stadig endring på grunn av masseforflytning fra isavsmelting i kryosfæren og geofysiske prosesser. Ved bruk av data fra gravimetrisatelliter kan disse variasjonene i jordas tyngdefelt bestemmes over en tidsserie.

Denne oppgaven prøver å gi en forklaring på hvordan jordas tyngdefelt forandres globalt og regionalt ved bruk av data fra GRACE over en tidsperiode. Ved å sammenligne tre ulike GRACE-løsninger og ved bruk av SLR-observasjoner, har masseendringer over Grønnland blitt estimert. I tillegg har det blitt sett nærmere på de laveregrads sfærisk harmoniske koeffisientene, for å gi en forklaring på hvordan disse koeffisientene fra GRACE påvirker beregninger av jordens tyngdefelt.

GRACE-data har sin usikkerhet i de laveregrads sfærisk harmoniske koeffisienter. C_{20}-koeffisientene fra GRACE har store varianser og må derfor bli byttet ut med SLR-verdier når man ser på globale variasjoner. Trendberegninger viser hvordan postglasial landheving(GIA) påvirker områdene Canada og Fennoskandia, og i tillegg issmelting over Grønnland, Alaska og Antarktis.

Ved å se nærmere på de laveregradskoeffisientene kan det bli observert at det ikke er av stor betydning hvordan man behandler C_{20}-koeffisienter når masseendringer over Grønnland blir estimert.

På grunn av begrenset romlig oppløsning og romlig glatting av tyngdefeltsmodeller, er det vanskelig å gi et realistisk estimat av masseendringer over et område. Dette blir kalt "leakage"-effekt. "Leakage"-effekten har blitt estimert og gjenopprettet, og masseendringer over Grønnland har blitt beregnet til å være mellom -1832.76 km^3 og -2087.72 km^3, avhengig av hvilken modell som har blitt brukt.

Acknowledgement

This thesis represent my work during the last four months and the end of my student life at the Norwegian University of Life Sciences.

First I would like to give sincere thanks to my supervisor Christian Gerlach, for guidance and encouragement during the work on my thesis. He has also given me the opportunity to visit the Commission for Geodesy and Glaciology at the Bavarian Academy of Sciences and Humanities for seven weeks during my work, for that I am really thankful. I also would like to thank my second supervisor Bjørn Ragnvald Pettersen.

A great thanks to GeoForum for the allocation of a scholarship that made the travel to Munich possible.

Thanks to Krzysztof Sosnica at the University in Bern for providing covariance matrices and explanations regarding the SLR- and GRACE-solutions.

I would also like to thank my fellow students at the "Geomatics office", for support and laughter during the last four months.

Finally, I would like to thank my friends and family for endless patience and interest in my work. And a special thanks to my parents for helping me out whenever needed and giving me motivation, I am forever grateful.

Karoline Skår

Ås, May 2015

Contents

List of Figures

List of Tables

Chapter 1

Introduction

The German geodesist Friedrich R. Helmert(1880) described geodesy as the *science of measurement and mapping of the Earth's surface*, this definition includes the determination of the Earth's gravity field, and is still valid today. The determination of Earth's physical properties is referred to as *physical geodesy*, and describes the shape, size and gravity field of the Earth. Because the Earth is rotating it cannot be a sphere, but more flattened and gives the Earth a more ellipsoidal shape. Gravity is mainly caused by the Earth's gravitational attraction, but also centripetal acceleration.

Gravity observations has been measured since the 18th century, and several different methods have been used. After the launch of the first satellites in the middle of the 20th century, global Earth observations has been carried out. With space based methods like Satellite Laser Ranging and dedicated gravity satellite missions like CHAMP, GRACE and GOCE the gravity field of the Earth can be determined.

1.1   Motivation

The Earth's gravity field is in constant change, due to mass redistribution on the Earth's surface. Melting of the large ice caps are of big interest when looking at climate change and how the rapid melting are affecting the Earth. Satellite missions for measuring changes in the Earth's surface has become a good and reliable method for looking at the changes in a global scale as well as for regions, i.e. Greenland and Antarctica. The Gravity Recovery and Climate Experiment(GRACE) mission has provided a time series of the global gravity field observations since more than a decade and gives good solutions for the global gravity field. This means that trends and variations can be estimated on a global and regional scale.

1.2   Objective

The aim of this thesis is to analyze published gravity field models from GRACE satellite mission and use these models to investigate the mass variations in the cryosphere when looking at a specific area or region. In the case of this thesis the area that will be studied is Greenland. While keeping in mind the variations over a specific area, the global mass changes will be investigated as well as looking in to spatial averaging of the gravity field models. The lower degree coefficients needs to be investigated even further: how they influence the global gravity field and how they influence Greenland when looking at the trend. A comparison between different solutions will be carried out when investigating the global gravity field variations, the lower degree spherical harmonic coefficients and of course the mass balance over Greenland.

1.3   Summary

A short summery of the chapters in this thesis will be given below:

Chapter 1: Introduction: This chapter gives the motivation for this thesis, thesis objective and a list of abbreviations used in the text.

Chapter 2: The gravity field of the Earth: This chapter gives the theory related to physical geodesy; Earth's gravity field and potential theory. The determination of gravity is described and how it is possible to use spherical harmonic synthesis to give a global gravity field. At the end of this chapter, some geophysical signals will be explained.

Chapter 3: Methods and technology: This chapter are describing different satellite methods that measures Earth's gravity field and gives an overview of different GRACE-derived gravity solution.

Chapter 4: Estimation of trend in the global gravity field solutions: This chapter explains the trend for the global gravity field. Estimation of trend is described, as well as de-aliasing and a comparison of the global gravity field solutions.

Chapter 5: Lower degree spherical harmonics: This chapter are investigating the lower degree spherical harmonics, and especially the C_{20}-coefficients. First the long term trend in the SLR-values are looked into. Then a comparison between the SLR values used in this thesis and how the C_{20}-coefficients influence the gravity field. A comparison between the C_{20}-SLR coefficients and the GRACE-derived C_{20}-coefficients is also given. At the end, an investigation of the trend in C_{20} and a short look into correlations of GRACE and SLR is carried out.

Chapter 6: Leakage effects: This chapter looks into the leakage effects over Greenland, and estimates mass changes over Greenland for the last decade.

Chapter 7: Concluding remarks and outlooks: This chapter gives the final conclusions of this thesis and outlooks.

1.4 Abbreviations

Abbreviation	Meaning
AIUB	Astronomisches Institut Universität Bern
AOD	Atmosphere and Ocean De-aliasing
CSR	Center for Space Research
DLR	Deutsches Zentrum Luft- und Raumfahrt
EOP	Earth Orientation Parameter
ESA	European Space Agency
EWT	Equivalent Water Thickness
GFZ	GeoForschungsZentrum
GIA	Glacial Isostatic Adjustment
GNSS	Global Navigation Satellite Systems
GPS	Global Positioning System
ICGEM	International Centre for Global Earth Models
IGS	International GNSS Service
ILRS	International Laser Ranging Service
ITRF	International Terrestrial Reference Frame
ITSG	Institute of Theoretical Geodesy and Satellite Geodesy
JPL	Jet Propulsion Laboratory
LEO	Low Earth Orbit
LLR	Lunar Laser Ranging
LOD	Length Of Day
NASA	National Aeronautics and Space Administration
RDC	GRACE Raw Data Center
SGG	Satellite Gravity Gradiometry
SLR	Satellite Laser Ranging
SST	Satellite-to-Satellite Tracking
TN7	Technical Note no. 7
VLBI	Very Long Baseline Interferometry

Chapter 2

The Earth's gravity field

Physical geodesy concerns the knowledge about the Earth's shape, size and gravity field. The Earth's geometrical characteristics and it's physical properties are closely tied together. With different observations it is possible to describe the Earth's gravity field globally.

2.1 Basic definitions

It starts with Newton's law of gravitation, with two masses attracted to each other with the force F and can be described as vector function

$$\vec{F} = F \cdot (-\frac{\vec{r}}{r}) = -\frac{GMm}{r^3}\vec{r} \tag{2.1}$$

F is the mutual force between the masses M and m separated by the distance r. G is universal gravity constant ($G = 6.67384 \times 10^{-11}$ m^{3}kg^{-1}s^{-2}) and $\vec{r}$ is the unit vector.

The gravitational force is given by $\vec{F} = m\vec{g}$, and this give the gravitational acceleration

$$\vec{g} = \frac{GM}{r^3}\vec{r} \tag{2.2}$$

In a conservative vector field, which means that there is no change in internal

energy balance, $\vec{g}$ can be described as the gradient to the scalar potential function V [Hofmann-Wellenhof and Moritz, 2006]

$$\vec{g} = \nabla V = \frac{\delta V}{\delta x}\vec{i} + \frac{\delta V}{\delta y}\vec{j} + \frac{\delta V}{\delta z}\vec{k} \qquad (2.3)$$

Earth's gravitational field can be proven to be conservative by showing that $curl(\vec{g} = 0)$. The vector representation in equation 2.3 can be described as function of the potential, V, and it is easier to work with the potential than three components of the force. The potential function is the sum of all the individual contributions

$$V = G \sum_{i=1}^{n} \frac{m_i}{r} \qquad (2.4)$$

where m_i is a series of several point masses $m_1, m_2, ..., m_i$. With the this continuous case the summation becomes an integral with a given density $\rho = \frac{dm}{dv}$, then the sum in (2.4) becomes an integral, *Newton's Integral*

$$V = G \iiint\limits_{Earth} \frac{dm}{r} = G \iiint\limits_{Earth} \frac{\rho}{r}\, dv, \qquad (2.5)$$

where dm is infinitesimal small elements of mass and volume, r is the distance between the mass element and attracted point [Hofmann-Wellenhof and Moritz, 2006].

Inside the Earth's surface, the potential V fulfills *Poisson's equation*

$$\Delta V = \frac{\delta^2 V}{\delta x^2} + \frac{\delta^2 V}{\delta y^2} + \frac{\delta^2 V}{\delta z^2} = -4\pi G\rho \qquad (2.6)$$

For point masses outside the Earth's surface, the density become zero and equation 2.6 can be written as *Laplace's equation*

$$\Delta V = \frac{\delta^2 V}{\delta x^2} + \frac{\delta^2 V}{\delta y^2} + \frac{\delta^2 V}{\delta z^2} = 0 \qquad (2.7)$$

The solutions of Laplace's equation, $\Delta V = 0$, is called *harmonic functions* and the gravitational potential will then be harmonic outside the attracting masses.

2.2   Boundary value problems

The Earth has been approximated to the sphere, but when boundary-value conditions are present the problem of solving Laplace' equation gets more complex.

Because we are working on a surface S, Dirichlet's problem, *the first boundary-value problem*, needs to be solved in order to obtain the potential V outside the surface. Dirichlet's problem is stated as follows; *the gravitational potential outside a surface S is determined by knowing the geometric shape of S and the potential on S* [Hofmann-Wellenhof and Moritz, 2006]. Dirichlet's problem can be solved for the sphere, and a solution is Poisson's integral

$$V_e(r, \theta, \phi) = \sum_{n=0}^{\infty} \left(\frac{R}{r}\right)^{n+1} \frac{2n+1}{4\pi} \int_{\lambda=0}^{2\pi} \int_{\theta=0}^{\pi} V(R, \theta, \lambda) P_n(\cos\psi) \sin\theta \; d\theta \; d\lambda \quad (2.8)$$

Other boundary-value problems are similar to the first boundary-value problem. *Neumann's problem* or the *second boundary-value problem* the normal derivative is given by $\partial V/\partial n$ on the surface S instead of the function V. For the *third boundary value problem* a linear combination of V and its normal derivative, $V + \partial V/\partial n$, is given on the surface S.

Neumann's problem can be expanded into a series of surface spherical harmonics. The harmonic function which solves Neumann's problem is

$$V_e(r, \theta, \lambda) = -R \sum_{n=0}^{\infty} \left(\frac{R}{r}\right)^{n+1} \frac{Y_n(\theta, \lambda)}{n+1} \quad (2.9)$$

The *third boundary value problem* is relevant because of the irregularities of the geoid from gravity anomalies, and can be solved by

$$V_e(r, \theta, \lambda) = R \sum_{n=0}^{\infty} \left(\frac{R}{r}\right)^{n+1} \frac{Y_n(\theta, \lambda)}{n-1} \quad (2.10)$$

2.3   Spherical harmonic representation

One of the most commonly used methods for the calculation of gravity field quantities is the *spherical harmonic synthesis*. Changes in the gravity field are dependent on the eigenvalues and the upward continuation factor used in the synthesis.

By summation of all solutions of Laplace's equation(2.7), a spherical harmonic representation can be obtained. For spherical coordinates the harmonic function of gravitational potential can be written as

$$V(r, \theta, \lambda) = \frac{GM}{r} \sum_{n=0}^{\infty} \left(\frac{R}{r}\right)^{n+1} \sum_{m=0}^{n} (\bar{C}_{nm} \cos m\lambda + \bar{S}_{nm} \sin m\lambda) \bar{P}_{nm}(cos\theta) \quad (2.11)$$

where $\bar{C}_{nm}$ and $\bar{S}_{nm}$ are the *fully normalized and dimensionless potential coefficients*, GM is the product between the gravitational constant and Earth's mass, and R is the mean Earth radius. $\bar{P}_{nm}(cos\theta)$ are the *fully normalized associated Legendre functions* and the subscripts n and m denotes the degree and order of the function. Figure 2.1 shows the Legendre functions for P_2, P_4 and P_6. The factor $(R/r)^{(n+1)}$ is called *upward continuation* and makes it possible to determine the potential outside the Earth surface, r is the geocentric distance.
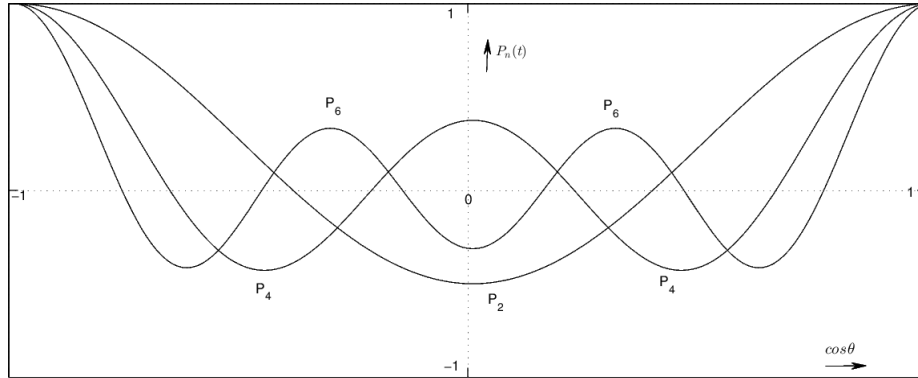
Figure 2.1: *Legendre polynomials for P_2, P_4 and P_6*

The Earth is rotating and therefore we need to operate with gravity potential:

$$W = V + V_c \tag{2.12}$$

where V is the gravitational potential and $V_c = 1/2\, \omega^2(x^2 + y^2)$ is the rotational potential [Hofmann-Wellenhof and Moritz, 2006]. Because the relations between the gravity potential and geodetic observations is not linear, an approximation of the gravity potential was introduced.

Gravity field modeling deals with the difference between the gravity potential and ellipsoidal potential, U (also called the normal potential), this potential difference can be expressed as disturbing potential, as shown in 2.13.

$$T = (W - V_c) - (U - V_c) = W - U \tag{2.13}$$

The disturbing potential is harmonic outside the masses. From Poisson we know that $\Delta V = -4\pi G\rho$, and from equation(2.12) it is possible to obtain

$$\Delta W = -4\pi G\rho + 2\omega^2 \tag{2.14}$$

Outside the masses the density is zero, then $\Delta V = 0$. And only the rotational contribution(ω) remains. The disturbing potential is then

$$\Delta T = \Delta W - \Delta U = 2\omega^2 - 2\omega^2 = 0 \tag{2.15}$$

The calculation of potential from amplitudes of the gravity field coefficients of signal gives the *spherical harmonic synthesis*. When subtracting the normal potential $\bar{U}_{nm}$ from the potential coefficients, spherical harmonic synthesis can be used to express the disturbing potential.

$$T(r, \theta, \lambda) = \frac{GM}{r} \sum_{n=2}^{\infty} \left(\frac{R}{r}\right)^{n+1} \sum_{m=0}^{n} (\Delta \bar{C}_{nm} \cos m\lambda + \Delta \bar{S}_{nm} \sin m\lambda) \bar{P}_{nm}(\cos \theta)$$
$$\tag{2.16}$$

where $\Delta\bar{C}_{nm}$ and $\Delta\bar{S}_{nm}$ are the residuals of the harmonic coefficients

$$\Delta\bar{C}_{nm} = \begin{cases} \bar{C}_{nm} - \bar{U}_{nm} & m = 0 \ \wedge \ n \in \{2, 4, 6, ..., N_{max}\} \\ \bar{C}_{nm} & else \end{cases}$$

(2.17)

$$\Delta\bar{S}_{nm} = \bar{S}_{nm}$$

The normal potential U is symmetric with respect to the equator and not dependent on the longitude λ. This gives that only the even zonal harmonics exist for the normal potential. Because sine-coefficients do not exist for $m = 0$, the sine coefficients are the same after subtracting the normal potential coefficients.

2.3.1   Legendre polynomials

It can be useful to look at the spatial representation of the spherical harmonics, and they can be divided into three categories, zonal, tesseral and sectorial. For the zonal harmonics, it holds m = 0 are only polynomials of degree n and have n zeros. They also do not depend on λ. If the order $m \neq 0$ ($m = 1, ..., n$), the Legendre polynomials are called *associated Legendre functions*. The tesseral harmonics make a square pattern when represented spatially. In the case where $n = m$ the functions divide the sphere into sectors, *sectorial harmonics*, see figure 2.2 [Hofmann-Wellenhof and Moritz, 2006]. For spherical harmonic degree $2 - 5$ $P_n (cos\theta)$ can be expressed as

$$P_2(cos\theta) = \frac{3}{4} \cos \ 2\theta + \frac{1}{4},$$
$$P_3(cos\theta) = \frac{5}{8} \cos \ 3\theta + \frac{3}{8} \cos \ \theta,$$
$$P_4(cos\theta) = \frac{35}{64} cos \ 4\theta + \frac{5}{16} \cos \ 2\theta + \frac{9}{64},$$
$$P_5(cos\theta) = \frac{63}{128} \cos \ 5\theta + \frac{35}{128} cos \ 3\theta + \frac{15}{64} \cos \ 3\theta$$
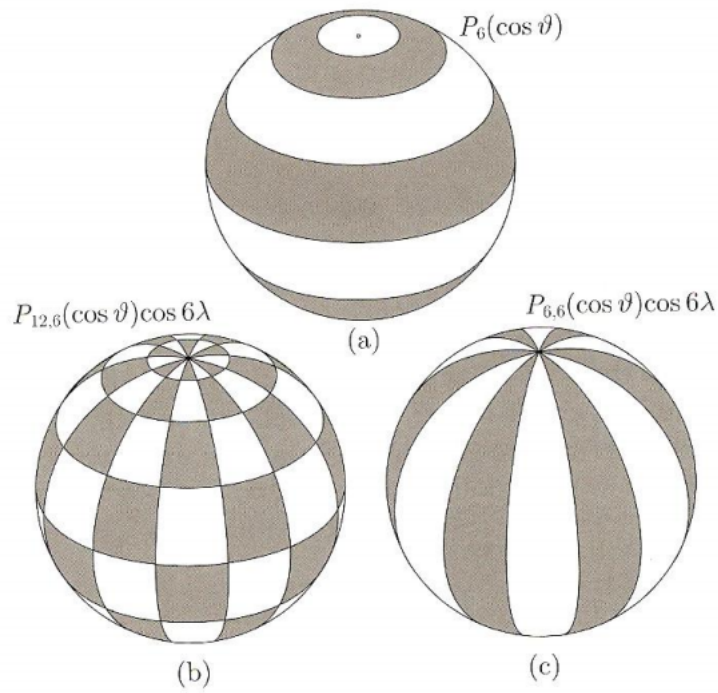
(2.18)

Figure 2.2: *Geometry of spherical harmonics. a) zonal, b) tesseral and c) sectorial. Figure from [Hofmann-Wellenhof and Moritz, 2006]*

2.4   Normal gravity field and disturbing quantities

There are different gravity quantities that can be calculated, disturbing potential T, geoid height N, gravity anomaly Δg and gravity disturbance δg. They are represented in table 2.1, and they differ by the spectral eigenvalues and the upward continuation factors. From this it is easy to convert between the different quantities.

T	$=$	$\frac{GM}{R}$	$\sum\limits_{n=2}^{\infty}$	$\left(\frac{R}{r}\right)^{n+1}$		$\sum\limits_{m=0}^{n}(\Delta\bar{C}_{nm}\cos m\lambda + \Delta\bar{S}_{nm}\sin m\lambda)\bar{P}_{nm}$
N	$=$	R	$\sum\limits_{n=2}^{\infty}$	$\left(\frac{R}{r}\right)^{n+1}$		$\sum\limits_{m=0}^{n}(\Delta\bar{C}_{nm}\cos m\lambda + \Delta\bar{S}_{nm}sinm\lambda)\bar{P}_{nm}$
Δg	$=$	$\frac{GM}{R^2}$	$\sum\limits_{n=2}^{\infty}$	$\left(\frac{R}{r}\right)^{n+2}$	(n - 1)	$\sum\limits_{m=0}^{n}(\Delta\bar{C}_{nm}\cos m\lambda + \Delta\bar{S}_{nm}\sin m\lambda)\bar{P}_{nm}$
δg	$=$	$\frac{GM}{R^2}$	$\sum\limits_{n=2}^{\infty}$	$\left(\frac{R}{r}\right)^{n+2}$	(n + 1)	$\sum\limits_{m=0}^{n}(\Delta\bar{C}_{nm}\cos m\lambda + \Delta\bar{S}_{nm}\sin m\lambda)\bar{P}_{nm}$
T_{rr}	$=$	$\frac{GM}{R^3}$	$\sum\limits_{n=2}^{\infty}$	$\left(\frac{R}{r}\right)^{n+3}$	(n + 1)(n + 2)	$\sum\limits_{m=0}^{n}(\Delta\bar{C}_{nm}\cos m\lambda + \Delta\bar{S}_{nm}\sin m\lambda)\bar{P}_{nm}$

Table 2.1: *Spherical harmonic synthesis of gravity field quantities.*

The summations in table 2.1 starts at $n = 2$. If we assume that the mass M and the radius R of the ellipsoid is equal to mass and the equatorial radius of the Earth, the zero degree term disappear. And if the center of Earth's masses coincides with the center of the ellipsoid, the first degree term will vanish as well [Torge and Müller, 2012].

The gravity field of the Earth is usually described in terms of the shape of the geoid [Wahr and Molenaar, 1998], and it is the sum of spherical harmonics

$$N(\theta, \lambda) = R\sum_{n=0}^{\infty}\sum_{m=0}^{n}\bar{P}_{nm}(\cos\theta)(\bar{C}_{nm}\cos\ m\lambda + \bar{S}_{nm}\sin\ m\lambda) \qquad (2.19)$$

where R is the Earth's radius, $\bar{P}_{nm}$ is the normalized associated Legendre functions and $\{\bar{C}_{nm}, \bar{S}_{nm}\}$ are the *fully normalized dimensionless coefficients*.

It can be assumed that there is a time dependent change in the geoid, ΔN. The change in geoid height can be represented in terms of changes in the spherical harmonic coefficients, $\Delta \bar{C}_{nm}$ *and* $\Delta \bar{S}_{nm}$

$$\Delta N(\theta, \lambda) = R \sum_{n=0}^{\infty} \sum_{m=0}^{n} \bar{P}_{nm}(\cos \theta)(\Delta \bar{C}_{nm} \cos\ m\lambda + \Delta \bar{S}_{nm} \sin\ m\lambda) \qquad (2.20)$$

The geoid change is caused by a redistribution in density, $\Delta \rho(r, \theta, \lambda)$, and it can be assumed that $\Delta \rho$ is concentrated as a thin layer at the surface of the Earth. The change in surface density can be defined as

$$\Delta \sigma(\theta, \lambda) = \int_{thin\ layer} \Delta \rho(r, \theta, \lambda) dr \qquad (2.21)$$

From this it is possible to separate the contribution of the coefficients into two components

$$\left\{ \begin{array}{c} \Delta C_{nm} \\ \Delta S_{nm} \end{array} \right\} = \left\{ \begin{array}{c} \Delta C_{nm} \\ \Delta S_{nm} \end{array} \right\}_{Surf\ Mass} + \left\{ \begin{array}{c} \Delta C_{nm} \\ \Delta S_{nm} \end{array} \right\}_{Solid\ Earth} \qquad (2.22)$$

The sum over (n,m) in equation 2.20 can be truncated to degrees $n < n_{max}$, and if the layer is thin enough that $(n_{max} + 2)H/a << 1$ (where H represent the thin layer), then $(r/a)^{l+2} \approx 1$. This gives the two components first stated in equation 2.22

$$\left\{ \begin{array}{c} \Delta C_{nm} \\ \Delta S_{nm} \end{array} \right\}_{Surf\ Mass} = \frac{3}{4\pi a_e \rho_{ave}(2n+1)} \int \Delta\sigma(\theta,\lambda)$$

$$\times \bar{P}_{nm}(cos\theta) \left\{ \begin{array}{c} \cos\ m\lambda \\ \sin\ m\lambda \end{array} \right\} sin\theta\ d\theta d\lambda \qquad (2.23)$$

and

$$\left\{ \begin{array}{c} \Delta C_{nm} \\ \Delta S_{nm} \end{array} \right\}_{Solid\ Earth} = \frac{3k_n}{4\pi a_e \rho_{ave}(2n+1)} \int \Delta\sigma(\theta,\lambda)$$

$$\times \bar{P}_{nm}(\cos\theta) \left\{ \begin{array}{c} \cos\ m\lambda \\ sin\ m\lambda \end{array} \right\} \sin\theta\ d\theta d\lambda \qquad (2.24)$$

To correct for the changes in potential caused by Earth tides, in the case of this thesis there is no connection to tides, however, in both cases k_n represents a scaling factor that describes the deformation of the solid Earth as function of the variable load and gravity field. The load Love numbers are dimensionless coefficients that are dependent on the degree of the spherical harmonics [Torge and Müller, 2012].

Equation 2.24 can be applied when calculating the spherical harmonic coefficients from coefficients in the spatial domain. This is a reverse spherical harmonic synthesis, also called *spherical harmonic analysis*. From the equations above we obtain

$$\left\{ \begin{array}{c} \Delta C_{nm} \\ \Delta S_{nm} \end{array} \right\} = \frac{3\rho_w}{4\pi \rho_{ave}} \frac{1+k_n}{2n+1} \int \Delta\sigma(\theta,\lambda)$$

$$\times \bar{P}_{nm}(cos\theta) \left\{ \begin{array}{c} \cos\ m\lambda \\ \sin\ m\lambda \end{array} \right\} \sin\theta\ d\theta d\lambda \qquad (2.25)$$

Mass changes can be approximated by surface mass densities, and is also a function of the same coefficients in equation 2.11

$$\Delta\bar{\sigma}(\theta,\lambda) = \frac{2\pi a_e \rho_{ave}}{3} \sum_{n=0}^{n_{max}} \frac{2n+1}{1+k_n} \sum_{m=0}^{n} \bar{P}_{nm}(\cos\theta)$$

$$\cdot(\Delta\bar{C}_{nm}\cos\ m\lambda + \Delta\bar{S}_{nm}\sin\ m\lambda) \qquad (2.26)$$

to determine the Equivalent Water Thickness(EWT) from surface mass densities, the simple relation is

$$\Delta\bar{v}(\theta,\lambda) = \frac{\Delta\bar{\sigma}(\lambda,\theta)}{\rho_w} \qquad (2.27)$$

In equation 2.26 a_e is Earth's semi-major axis, $\rho_{ave} = 5517 kg/m^3$ is the average mass density of the Earth, ρ_w=1000 kg/m^3 the density of water and k_n is the load love numbers [Wahr and Molenaar, 1998]. W_n is the spatial averaging function(i.e Gaussian smoothing), and will be described and used in chapter 4 and 6.

2.5   Statistics for the gravity field

Describing the Earth statistically is useful to get an idea of the quality of measurements and the methods that has been applied. The variance is of good use to look at the accuracy of the gravity anomalies of the Earth. A global variance for gravity anomaly is given

$$\sigma^2(\Delta g) = M\{\Delta g\} = \frac{1}{4\pi}\iint_{\sigma}\Delta g d\sigma \qquad (2.28)$$

where M is the average over the whole globe, *the global mean function.* The dimensionless degree variance are given by

$$c_n = \sum_{m=0}^{n}\left[\Delta\bar{C}_{nm}^2 + \Delta\bar{S}_{nm}^2\right] \qquad (2.29)$$

where ΔC_{nm} and ΔS_{nm} are the spherical harmonic coefficients. From table 2.1 the gravity anomaly is given, and from this it is possible to derive the signal variance for gravity anomaly

$$\sigma^2(\Delta g) = \sum_{n=2}^{\infty} \sum_{m=0}^{n} \left[\left(\frac{GM}{R^2}(n-1)\Delta \bar{C}_{nm} \right)^2 + \left(\frac{GM}{R^2}(n-1)\Delta \bar{S}_{nm} \right)^2 \right]$$

$$= \sum_{n=2} c_n^{\Delta g} \tag{2.30}$$

With the use of spectral eigenvalues and scaling factors, it is possible to obtain the degree variances for i.e gravity anomaly(2.31) and geoid height(2.32)

$$c_n^{\Delta g} = \sum_{m=0}^{n} \left(\frac{GM}{R^2}(n-1) \right)^2 \cdot \left[\Delta \bar{C}_{nm}^2 + \Delta \bar{S}_{nm}^2 \right] \tag{2.31}$$

The same computations can be done for the geoid height, and are given as

$$c_n^{\Delta N} = R^2 \sum_{m=0}^{n} \left[\Delta \bar{C}_{nm}^2 + \Delta \bar{S}_{nm}^2 \right] \tag{2.32}$$

Different models for degree variances has been carried out, when it was found out that the different potential models had quite similar degree variances. This is because most of the potential models describes the same gravity field. Kaula and Tscherning/Rapp has carried out theoretical degree variance models, where Kaula's model(2.33) is based on the potential coefficients, while Tscherning/Rapp is based on gravity anomalies(2.34).

$$c_n = 0.5 \frac{1.6 \times 10^{-10}}{n^3} \qquad n > 0 \tag{2.33}$$

$$c_n^{\Delta g} = s^{n+2} \frac{A(n-1)}{(n-2)(n-B)} \qquad n \geq 3 \tag{2.34}$$

where A = 425.28 $mGal^2$, B = 24 and s = 0.999617. To avoid singularity n start at degree 3, and degree 2 is equal to 7.5 $mGal^2$.

The degree variances are useful for comparison of signal content in different sets of coefficients. Because of the similarity between the different models, it can be more useful to compute *error degree variances*. This means that the computation of degree variances is done by standard deviations of the coefficients. From a plot that contains both signal degree variances and error degree variances it is possible to determine the resolution of the model. The resolution is found where the degree variance and the error degree variance intersects, and the signal to noise ratio is equal to 1. Above this point the noise is greater than the signal itself.

From the error in the coefficients it is also possible to calculate the commission- and omission error. The commission error describes the error standard deviation up to the maximum degree, and the omission error describes the signal content above the maximum degree.

2.6   Gravity variations and geophysical signals

There are several geophysical signals that vary over time and cause temporal variations of the global and regional gravity field. More regional effects are tidal loading(atmospheric pressure loading, solid, earth tides, ocean tide, ocean tide loading), post glacial rebound and hydrology- and cryospheric variations(Non-tidal loading effects). This section looks further into some of these gravity variations.

2.6.1   Earth's rotation

The gravity potential consists of gravitational potential and the rotational potential, described in equation 2.12. Earth's rotation can be described by a vector directed to the north pole and by the angular velocity ω. The magnitude and the direction of the vector that represent the rotational axis are changing in time with respect to the solid Earth. This is due to both external gravitational processes and geodynamical processes.

Changes in Earth's rotation will influence the gravity of the Earth, and the magnitude of gravity can be expressed as

$$g = |\nabla W| \tag{2.35}$$

The acceleration of gravity can be expressed in spherical coordinates

$$|\nabla W| = \sqrt{(V + \Phi r)^2 + \left[\frac{1}{r cos\phi}(V_\lambda + \Phi_\lambda)\right]^2 + \left[\frac{1}{r}(V_\phi + \Phi_\phi)\right]^2} \tag{2.36}$$

where V is the gravitational potential and Φ is the centrifugal potential. The subscripts denote the partial derivatives with respect to each of the spherical coordinates [Barthelmes, 2009]. Further, the rotational potential can be described as

$$\Phi = \frac{1}{2}\omega^2 r^2 (cos\phi)^2 \tag{2.37}$$

Observations of the Earth rotation parameters gives information about the Earth's interior properties and mass transport in atmosphere, oceans, mantle and core. The rotation and the orientation axis of the Earth is reason to irregular variations [Torge and Müller, 2012].

The Earth's rotation can be described by the Earth Orientation Parameters notably called EOP. EOP describes the irregularities of the rotation of the Earth, and consist of determination of length of day(LOD) and the coordinates of the pole(X,Y). These parameters lies within the determination of the lower degree coefficients ΔC_{21} and ΔS_{21}, and Chen et al. finds an agreement between the degree 2 spherical harmonic coefficients and estimates from Earth rotation and climate models.

2.6.2   Polar motion

The Earth's rotational axis is not fixed, but small variations are observed. The polar motion refers to the motion of the Earth's spin axis with respect to the Earth fixed reference system. This motion occurs because of the minute difference between the axes of rotation and maximum inertia; the angle between them is about 0.3". The period of the polar motion is about 430 days, and is named *the Chandler period*. This period is also irregular due to movement of masses and atmospheric variations over the whole globe [Hofmann-Wellenhof and Moritz, 2006]. The polar motion is measured relative to the mean epoch of the ITRF. Since the 1980's space geodetic observations like VLBI[1], SLR and LLR[2] has been used to measure the polar motion. When global navigation systems was introduced in the 1990's the precision of the daily position of the pole yields $\approx$ 0.03 mas[3], that is approximately 1 mm on Earth's surface[Chen et al., 2013].

---

[1]Very Long Base Line Interferometry
[2]Lunar Laser Ranging
[3]milliseconds of arc

The perturbation in the potential V are given by

$$V_c(r, \theta, \lambda) = -\frac{\omega^2 r^2}{2} sin2\phi(m_1 cos\lambda + m_2 sin\lambda) \tag{2.38}$$

where ω is the angular velocity, r is the radial distance, θ and λ are the position, and m_1 and m_2 are the discrepancy between the location of the axis an the mean location of the axis

$$m_1 = x_p - \bar{x}_p \tag{2.39}$$
$$m_2 = -(y_p - \bar{y}_p) \tag{2.40}$$

Since the gravity potential is dependent on both the gravitational potential and the rotational potential, the polar motion needs to be taken into account when calculating gravity potential of the Earth.

Figure 2.3 displays the polar motion since 2001 and the mean pole displacement since 1900. As seen in the figure the polar motion are perturbed and has a spiral curve. The drift in mean pole is also irregular and shows westward motion.
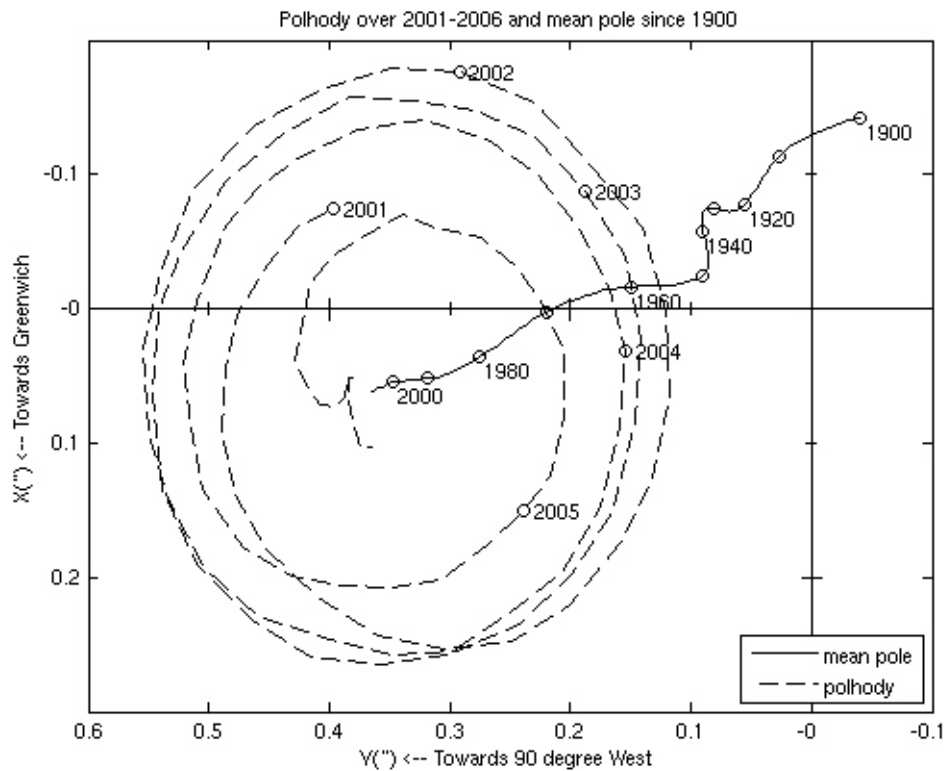
Figure 2.3: *Polar motion. Illustration: NASA*

The polar motion is affected by the Earth's mass redistribution(e.g post glacial rebound), and Chen et al.(2013) finds a close connection between the long term polar motion and mass redistribution, due to climate changes, by using GRACE-data. Because of the increased ice melting rates, that causes an eastward motion of the mean pole, the IERS[4] has started using higher order polynomial to define the mean pole.

2.6.3   Post-glacial rebound

Post-glacial rebound is the adjustment of the Earth surface due to the last ice-age, and is also named *Glacial Isostatic adjustment(GIA)*. The deglaciation cycle, that started about 21,000 years ago, is causing the Earth's crust to adjust back to the hydrostatic equilibrium. In Fennoscandia and Canada a land uplift is occurring

---

[4]International Earth Rotation and Reference system Service

due to the effect of GIA. This post glacial effect also has an impact on Earth rotation, sea level changes and gravity field variations [Torge and Müller, 2012]. In figure 2.4 the dynamics of the GIA-effect is visualized. Because of the Earth's viscoelasticity the ice pushed the crust and mantle down, when the ice melts the mantle flows back and causing the land to lift back to equilibrium.
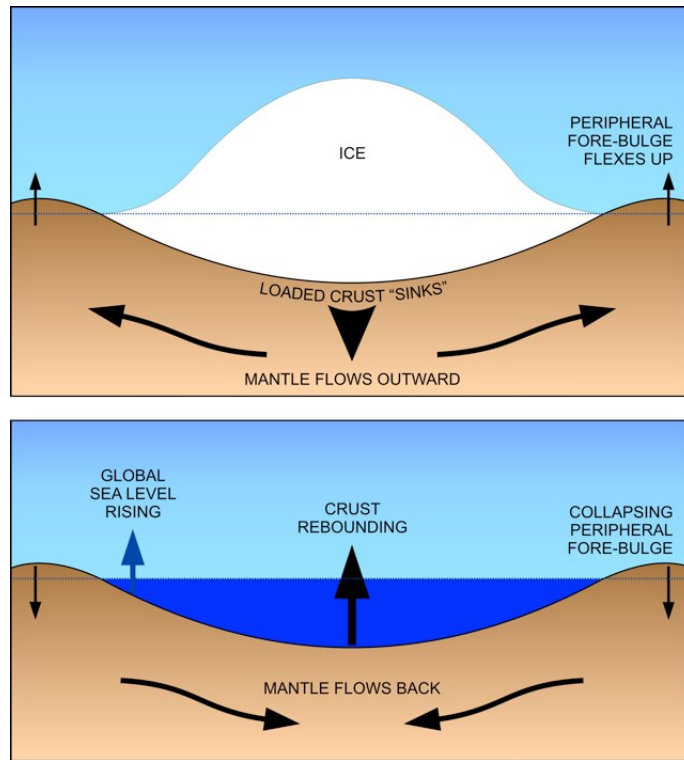
Figure 2.4: *Illustration of the GIA-effect. Illustration: Canadian Geodetic Survey*

Measurement and observations as leveling, sea level data, GPS and gravimetry has been used to measure the uplift. From leveling an uplift of rates up to 9 mm/yr has been observed and confirmed by GPS-measurements [Torge and Müller, 2012].

Different models have been derived from multiple observational methods, and these models are taking the mantle viscosity and thickness into account. Some models provides history data for sea level changes relative to the Earth that is deforming(e.g. ICE-5G).

Due to GIA, the Earth's gravity field will be affected by the mass redistribution, and temporal changes occurs when the masses in the Earth's mantle are retreating to the areas where it has previously been an ice sheet.

2.6.4 Tidal and loading effects

The solid Earth is affected by Earth tides caused by the gravity of the moon and the sun, and are causing gravity changes and deformation of Earth's surface. The Earth reacts to these effects like an elastic body. The effects on the Earth are called tidal loading, and consists of oceanic and atmospheric tides. Locally mass variations emerges from the solid Earth tides, and the geocentric distance from Earth's center of mass are increased.

Tides in the ocean are due to the attraction of the water masses and their loading effects on the Earth's surface, and contribute to approximately 70% of the sea surface [Torge and Müller, 2012]. The mass variations over the oceans and near the coastlines are caused by ocean tides. Since gravity is dependent on the mass, the local tidal variations needs to be implemented. Ocean loading is due to the mass variations in the ocean tides, and are a secondary tidal effect [Subirana et al., 2011].

The atmospheric loading comes from atmospheric tides and currents in the atmosphere. Changes in gravity due to direct an indirect loading effects, comes from the effect of atmospheric pressure changes. The variation in pressure results in a deformation of the Earth's surface, and are called atmospheric pressure loading [Petrov and Boy, 2004].

2.6.5   Non-tidal loading effects

In addition to the geophysical effects mentioned, non-tidal loading effect also affects the gravity variations of the Earth. These effects are due to mass redistribution in

- atmosphere

- ocean

- continental hydrology

- cryosphere

- earthquakes

- post glacial rebound

70% of Earth's surface are covered by water, and contributes to mass displacements. Ocean currents leads to temporal variations in the gravity field, but also groundwater can affect the gravity variations and are mainly caused by local weather(e.g rainfall). These effects causes a change in ocean bottom pressure and is called *non-tidal ocean loading*, and also takes changes in atmospheric pressure over the oceans into account.

Large areas of the Earth consist of water in solid state, the cryosphere. Melting of ice causes mass redistribution, and affects the global gravity field. To isolate i.e ice mass changes, one has to reduce atmospheric mass changes and solid earth mass displacements due to GIA.

Chapter 3

Methods and technology

3.1 Satellite Gravimetry

The first satellites were launched in the middle of the 20th century and made it possible to make global Earth observations. The geodetic observation techniques opened up for making gravity field covering the Earth. Satellite Laser Ranging and satellite altimetry gave a spatial resolution of half a wavelength, ≈ 500 km [Seeber, 2003]. With this resolution it was possible to obtain a spherical harmonic degree of ≈ 36, and an accuracy of the geoid to 1 meter. Dedicated satellite missions, such as GRACE, GOCE and CHAMP have improved the accuracy of the global gravity field models. Because of the Earth's irregularity in the gravitational field, the satellite is susceptible to perturbing forces. These forces are observed as "free fall" and from this it is possible to derive the gravity field of the Earth.

To be able to determine the global gravity field with high accuracy, low earth orbiting satellites(LEO) with sensitive sensors are required. This can be achieved with satellite-to-satellite tracking(SST) and satellite gravity gradiometry(SGG). SST uses microwaves to measure the range and range rates between two satellites. Satellites in high-low mode are tracked by GNSS satellites orbiting at a higher altitude(e.g. CHAMP), and is connected to a network of ground stations. With low-low mode two LEO satellites are placed in the same orbit separated with approximately 200 km(in case of GRACE) and the range between the two satellites is measured with high accuracy. Satellite gradiometry measures the gravity differences within the satellite(e.g. GOCE). The satellite is in free fall and therefore

the accelerations have to measured a distance from the center of mass of the satellite [Torge and Müller, 2012]. Figure 3.1 shows the concepts dedicated satellite gravity field missions.
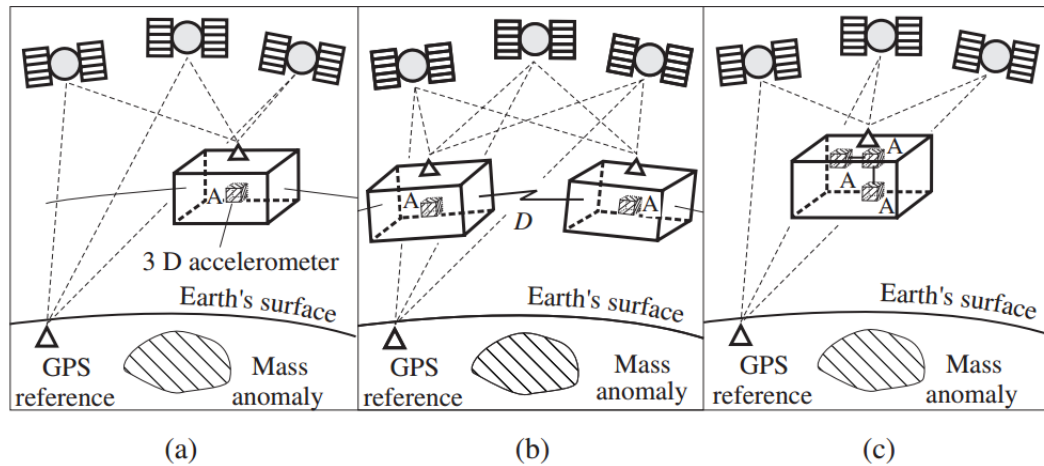
Figure 3.1: *Concepts of satellite gravity field missions. a)SST-HL, b) SST-LL, c) SGG Illustration: Seeber 2003, Satellite Geodesy, p. 471, figure 10.2*

Through satellite missions like GRACE, GOCE and CHAMP the spatial resolution and accuracy has improved. And with data from these satellite missions, including SLR, the best global gravity field models are obtained. In the following section a further description of SLR, CHAMP, GRACE and GOCE will be explained.

3.1.1 SLR – Satellite Laser Ranging

In 1964 the first satellite carrying reflectors was launched, the BEACON EXPLORER-B, but the development of pulsed laser systems for tracking satellites started in 1961 in USA [Seeber, 2003]. Over the years the Satellite Laser Ranging systems has developed from having an accuracy at over a meter down to an accuracy of some millimeters. It should be noted that the range accuracy is correlated with the length and the resolution of the laser pulse.

SLR measures the time it takes for a laser pulse to travel between a ground station and a satellite. A laser pulse is generated in the ground station and is transmitted to the satellite that carries retro-reflectors. The reflected pulse is then received at the ground station and the distance can be found by the simple observation equation

$$d = \frac{\Delta t}{2} c,$$

where c is the speed of light, Δt is the travel time of the laser pulse.

Dedicated satellites with retro reflector have been developed to give a higher accuracy of the Earth's gravity field and orbital parameters. Satellites dedicated for this purpose are STARLETTE, STELLA, LAGEOS-1 and -2, ETALON-1 and -2, GFZ-1 and WESTPAC [Seeber, 2003].

SLR has several fields of applications, and the main applications are:

- **Gravity field and satellite orbits:** SLR can determine low degree and order coefficients with high accuracy and precise determination of orbits

- **Positions and reference frames:** SLR can give absolute geocentric coordinates, heights and contributes to ITRF[1]

- **Earth Orientation Parameter:** SLR can determine polar motion and variations in Earth rotation

Laser ranging is organized under the International Laser Ranging Service(ILRS) and provides precise geocentric position, motion of ground stations, satellite orbits, Earth's gravity field and temporal variations and the Earth Orientation Parameters(EOP). ILRS collect and analyze laser ranging data from the 43 ground station distributed over the globe.

SLR has been providing data of the Earth's gravity field with high accuracy ever since the first satellites with retro reflectors was launched. SLR still plays an important role in estimating the global gravity field of the Earth, with the long time series of observations. SLR is especially valuable for the determination of the lower degree spherical harmonics, and is often an asset to other gravity field models derived from gravity satellites, and will continue to be a part of gravity field modeling.

---

[1]International Terrestrial Reference Frame

3.1.2   CHAMP – CHAllenging Minisatellite Payload

CHAMP was launched 15 July 2000 and Geoforschungszentrum Postdam has the
main responsibility for the mission and the mission ended September 19 2010.
The main goals of the CHAMP satellite mission was mapping of the global gravity
field and temporal variations, mapping the global magnetic field and profiling of
the ionosphere and the troposphere [Hofmann-Wellenhof and Moritz, 2006]. The
CHAMP satellite had an almost circular, near polar orbit with an inclination of
87°and an initial altitude of 454 km. The satellite had a lower orbit because of the
atmospheric drag, the lower altitude increased the sensitivity to Earth's gravity
field and determination of the coefficients. The magnetometer measures the vector
components of the magnetic field of the Earth and was separated from the body of
the aircraft, due to 'magnetic cleanliness' [GFZ, 2014]. The payload also consisted
of GPS receivers to determine the orbit, but also laser reflectors for tracking and
precise orbit determination. In addition the satellite had three-axis accelerometer
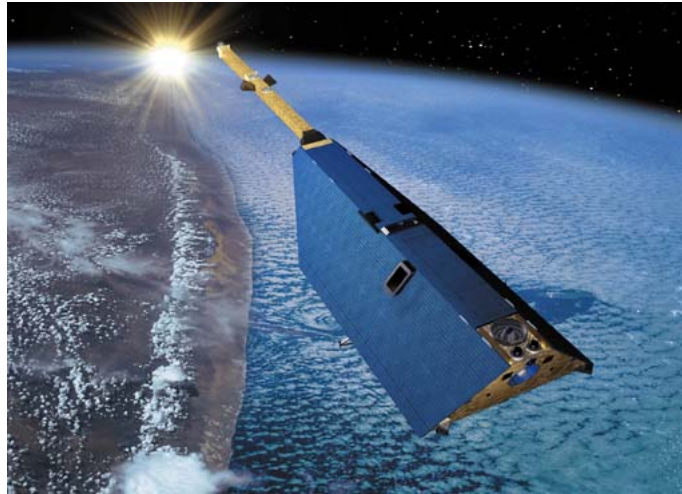to determine the non-gravitational accelerations(i.e air drag and solar radiation).

Figure 3.2: *CHAMP-mission Illustration:Airbus Defence and Space*

3.1.3 GRACE – The Gravity Recovery and Climate Experiment

The Gravity Recovery and Climate Experiment, GRACE, is a project between U.S National Aeronautics and Space Administration(NASA) and the German Aerospace Center(DLR). The GRACE-mission has made high resolution gravimetry measurements from space available and since 2002 GRACE has provided monthly global gravity solutions.

The GRACE-mission consists of two twin satellites(GRACE-A and GRACE-B) that have a range of approximately 220 kilometers, and are Low Earth Orbiting (LEO) satellites with an altitude of 490 km and a near polar orbit with an inclination at 89°. GRACE obtain Earth's gravity field by accurate measuring of the distance between the two satellites by using microwave systems. The distance change between the two satellites are measured with K-band ranging, and has an accuracy within $10\mu m$. The GPS receiver gives precise orbit determination of the satellites, and also provides data of atmosphere and ionosphere. As stated earlier, to achieve high resolution of the Earth's gravity field, LEO-satellites are required. The GRACE mission fulfills these requirements, operating in SST low-low mode, and the twin satellites have the same orbit [Torge and Müller, 2012].
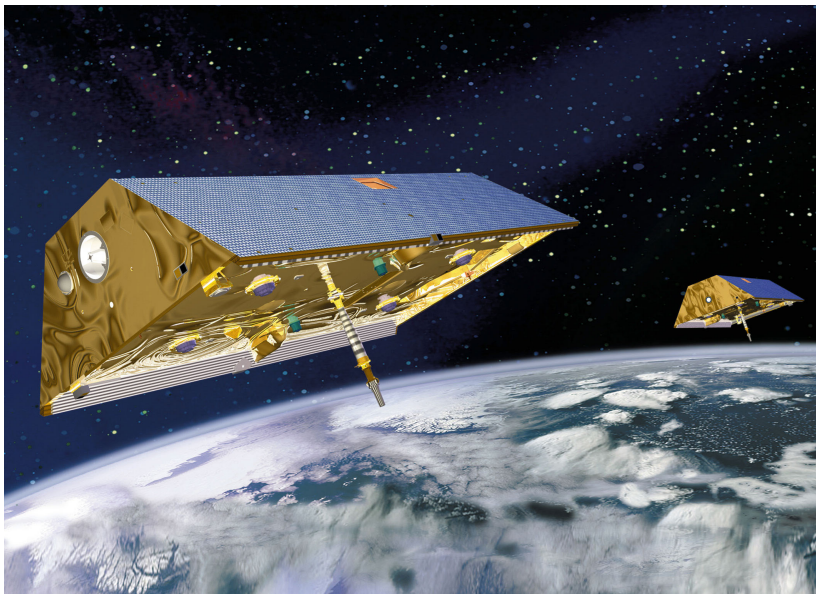

Figure 3.3: *The Gravity Recovery and Climate Experiment - GRACE, twin satellites [NASA, 2015]*

With constant measuring of the distance between GRACE-A and -B it is possible to determine the Earth's gravity field. The satellites are influenced by Earth's masses and when a mass anomaly occurs, an perturbation of the orbit will take place, and the distance between the satellites changes. From this change is is possible to derive models of Earth's gravity field. The spacecraft is also influenced by other non-gravitational accelerations, to determine this an accelerometer is used.

The objective of the GRACE-mission is to determine global high-resolution gravity fields and temporal variations. Because of atmospheric drag, the altitude of GRACE is decreasing, and the satellite mission is expected to continue throughout 2015. A GRACE follow-on mission will be launched in 2017, and will continue to give high resolution gravity field models.

3.1.4 GOCE – Gravity field and steady-state Ocean Circulation Explorer

The GOCE-mission is a part of ESA's The Living Planet Programme with goal to measure Earth's stationary gravity field with high accuracy. GOCE was launched 17 March 2009 and measured the Earth's gravity field until 11 November 2013. The mission objectives can be summarized to

- determine gravity anomalies with an accuracy of $1mGal(=10\mu m/s^2)$

- determine the geoid with an accuracy of 1-2 cm

- achieve these results at a spatial resolution better than 100 km

According to the mission requirements GOCE was intended to represent the gravity potential by spherical harmonics up to at least degree 200 [Hofmann-Wellenhof and Moritz, 2006].
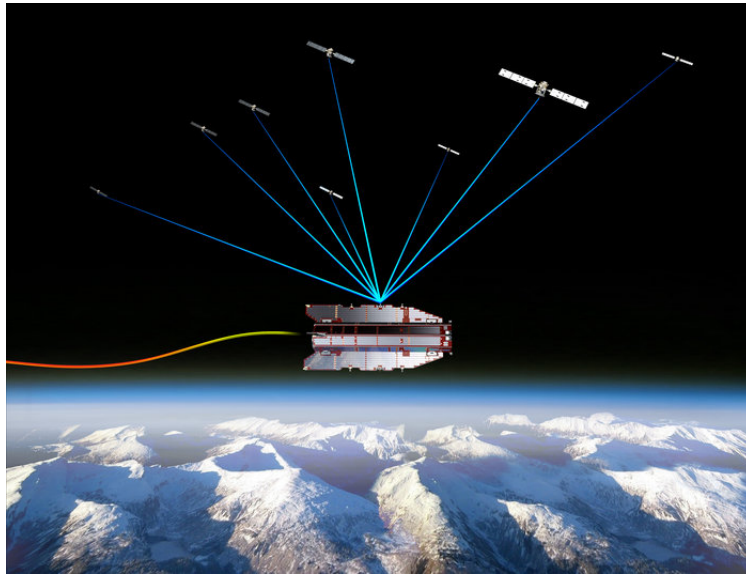
Figure 3.4: *GOCE satellite mission, illustration: ESA*

GOCE was a near-circular, low earth orbiting(LEO) satellite with an altitude of approximately 250 km and an inclination of 96.7°. The reason for the low altitude was to give as strong as possible gravity field signal. The main instrument on the GOCE-satellite was Electrostatic Gravity Gradiometer(EGG), or Satellite Sravity Gradiometer(SGG) that measured gravity gradients in all directions. The satellite was designed for measuring the geoid and gravity anomalies. The gradiometer consisted of six 3-axis accelerometers mounted in a diamond configuration. GOCE had two GPS receivers on the wing that was faced towards the space to supplement the gradiometer measurements. The orbit of the satellite was tracked by SLR that measured to the laser reflectors mounted on the satellite.

The data from the mission has been giving a better understanding of the Earth's geodynamics, ocean currents and heat transport, sea-level changes, give a global height reference system and give a better estimate of the thickness of the polar ice sheets and their movement.

3.1.5   Short summary of the gravity satellite missions

The three gravity satellite missions represented in this section has played a big role in the gravity field modeling of the Earth. They have all contributed to a better understanding of the global gravity field and its variations. Table 3.1 gives a short summary of the dedicated satellite missions.

Properties	GRACE	GOCE	CHAMP
Operator	NASA & DLR	ESA	GFZ
Launch Date	March 17 2002	March 17 2009	July 15 2000
Decay Date	Still in orbit	November 11 2013	September 19 2010
SST-mode	Low-Low	High-Low	High-Low
Altitude	500 km	250 km	300-450 km
Method	Orbit Perturbation	Gradiometry	Orbit Perturbation
Spatial Resolution	300 km	100 km	400 km

Table 3.1: *Summary of the different satellite gravimetry methods*

The GOCE mission gives gravity coefficients up to degree and order 250, but does not estimate the lower degree coefficients accurate enough for the purpose of this thesis where the focus is on the global time variations. This is why the use of GRACE is the method used to analyze the changes of Earth's gravity field over a long period of time, where GRACE have a higher accuracy of the lower degrees.

Figure 3.5 is presenting the differences between the satellite gravimetry methods in terms of degree variances. Satellite-to-satellite tracking Low-Low, denoted as SST-ll in the figure, is representing the GRACE-mission, SST-hl is the high-low method and representing the CHAMP-mission, while SGG is the satellite gravity gradiometry representing the GOCE-mission. In addition the Kaula model has been added to the figure, as well as GMs that is global models from before the life of GRACE, GOCE and CHAMP. Satellite Gravity Gradiometry, or GOCE, has a smaller variance in the coefficients for the higher degree spherical harmonics compared to GRACE(SST-ll), represented as a yellow field in the figure. For the

lower degree spherical harmonics, and the one that is the most applicable for the
purpose of this thesis, the GRACE-solution shows a smaller variance compared to
the GOCE-solution(represented as orange area in the figure).

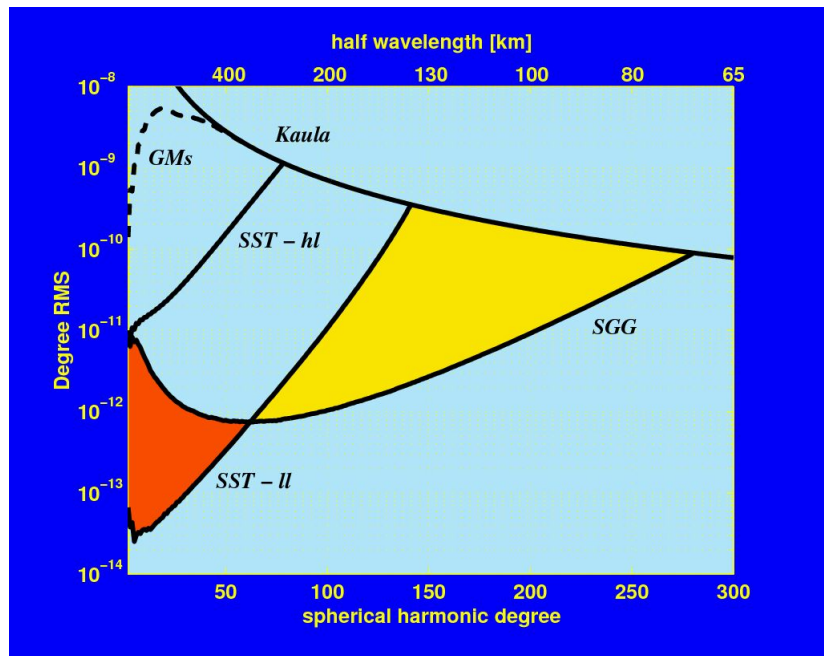**Figure 3.5:** *Comparison of degree variances between different methods: SST-LL, SST-HL, SGG and the Kaula-model*

The next dedicated satellite mission to be launched is the GRACE follow-on(GRACE-
FO) mission that will be launched in 2017, and will continue the modeling of
Earth's gravity field. GRACE-FO is a partnership between NASA and GFZ and
the goal is to obtain global and high resolution for the Earth's gravity field [GFZ,
2015].

3.2 GRACE Gravity Solutions

GRACE provide accurate estimates of the Earth's gravity field, and are used in several different analysis: mass redistribution, ocean and hydrological analysis, temporal variations in the Earth's gravity field etc. GRACE monthly solutions are mainly obtained from the three processing centers GFZ, JPL[2] and CSR[3], but also other groups/universities provides monthly GRACE solutions. The International Center for Global Earth Models(ICGEM) provides the data from the different models available.

This section will take further look in to the models from GFZ, ITSG and AIUB, the models used in this thesis. For all global gravity field models, monthly solution up to degree and order 90 has been used.

3.2.1 GFZ - German Research Center for Geosciences

The German Research Center for Geosciences is a national research center for Earth Sciences in Germany. GFZ provides gravity field solutions from GRACE at level-1B and level-2. Monthly solutions from January 2003 to July 2014 can be obtained, and their latest release are RL05a. The difference between the former release, RL05, and the latest release, is the difference in treatment of the orbit parameters in the final processing step, when the gravity field parameters are estimated. [Dahle et al., 2012]

GFZ provides a set of files that contains different information. The list below describes the different models that can be obtained.

- GSM - Static field geopotential coefficients estimated from satellite data only. These coefficients have had the modeled estimated of the atmospheric and oceanic mass signals removed.

- GAA - Non-tidal atmosphere geopotential coefficients averaged over a certain time period.

- GAB - Non-tidal ocean geopotential coefficients averaged over a certain time period.

---

[2]Jet Propulsion Laboratory
[3]University of Texas at Austin, Center for Space and Research

- GAC - Non-tidal atmosphere and ocean geopotential coefficients averaged over a certain time period.

- GAD - Ocean bottom pressure geopotential coefficients averaged over a certain time period.

For the generation of gravity field products at level-2, GFZ uses a two-step method:

1. adjustment of the high flying GPS spacecraft orbit and clock parameters from ground based tracking data.

2. determination of GRACE orbit and computation of the observation equtions with fixed GPS spacecraft.

For the computation of the GRACE level-2(explained in section 4.1) data, GFZ has used level-1B instrument data from release 02, and non-tidal atmosphere and ocean corrections from AOD1B product release 05 has been used. Release 05 level-2 products are generally generated up to degree and order 90, and are without any statistical constraints. The solutions are stabilized for selected months where there have been limitations in the ground track coverage due to repeat or nearby repeat orbit pattern.

3.2.2   AIUB - Astronomic Institute, University in Bern

AIUB has since 1992 operated the Center for Orbit Determination in Europe(CODE), and contributes to the International GNSS Service as an analysis center, as an analysis center to the International Permanent Network(EPN) and as an analysis center for the International Laser Ranging Service(ILRS). They provide data that contribute to the International Terrestrial Reference Frame(ITRF)

- Earth Rotation Parameters

- Precise satellite orbits and station coordinates

- Satellite and receiver clock corrections

- Global ionosphere maps and station troposphere parameters

AIUB provides monthly solutions from March 2003 to March 2013 , their newest release is the AIUB-GRACE03s. The static coefficients has been estimated up to degree and order 160, in the course of generalized orbit adjustment procedure. From the static part, monthly gravity field solutions has been estimated up to degree and order 60 and 90. The coefficients were computed from kinematic GPS position and low-low K-band inter satellite range rate observations [U. Meyer, 2011].

AIUB also provides monthly SLR solutions up to degree and order 10. The lower degree SLR-values will be investigated further in section 5.2.

3.2.3 ITSG-GRACE2014 - Institute for Theoretical geodesy and Satellite geodesy, Graz

ITSG provides monthly solutions for different maximum degrees, 60, 90 and 120 For this thesis a maximum degree of 90 has been used. The timespan is from February 2003 to June 2014. The observations for computing the coefficient are K-band range rates with sampling rate of 5 seconds, and kinematic orbits with sampling rate of 5 minutes. Each component in the solution contains complete gravity signal, with atmosphere and ocean masses [Mayer-Gürr et al., 2014].

They also provide a daily solution, where Kalman smoothing has been applied

Figure 3.2 shows an overview of the different solutions

Model name	Time Span	Spectral resolution
GFZ RL05a	April 2002 - September 2014	90
AIUB RL02	March 2003 - March 20013	60, 90
ITSG-GRACE2014	February 2003 - June 2014	60, 90, 120

Table 3.2: *Models from GFZ, AIUB and ITSG and their parameters*

Chapter 4

Estimation of trend in the global gravity field solutions

GRACE has delivered observations for monthly global gravity field solutions since its launch in 2002. This chapter will describe the computation of global gravity field changes with the use of GRACE-derived spherical harmonic coefficients in the spherical harmonic synthesis.

4.1 Data reduction and de-aliasing

Insufficient sampling rate of the temporal gravity field changes, causes aliasing in the GRACE gravity field models. This effect needs to be taken into account in order to derive the gravity field of the Earth from GRACE. Short-term variations as tides, atmospheric variations and oceanic variations are modeled and included in the back ground gravity field. This is called *atmospheric and oceanic de-aliasing(AOD)* and are reduced before the data are analyzed, so that the monthly solutions do not contain atmospheric- and oceanic variations.

This section will give a short description of the GRACE data products that are categorized into Level 0, Level 1A, Level 1B and Level 2.

4.1.1   Level 0

The level-0 data product consist of the observational raw data, and are processed by the GRACE Raw Data Center (RDC) at DLR. From each downlink pass of the satellites two files are made available and stored in the archives at RDC [Case et al., 2010].

4.1.2   Level 1A

Level-1A data product is a result of non-destructive processing of the level-0 data product. The processing include sensor calibration, ambiguity resolving and reformation of data. Sensor calibration factors are applied to convert the binary encoded measurements to engineering units. The level-1A data product are reversible to level-0 data products. This data product also include ancillary data that is needed for the processing of the next step [Case et al., 2010].

4.1.3   Level 1B

The level-1B data products are correctly time tagged, and are possible irreversible processing applied to level-0 and level-1A data. Level-1B data contains intersatellite range, range rate, range acceleration and non-gravitational accelerations from both GRACE-A and GRACE-B. This level also includes ancillary data that has been generated during the processing, and also data needed for further processing [Case et al., 2010]. GFZ provides an atmosphere and ocean de-aliasing product for level 1B, called AOD1B.

4.1.4   Level 2

The level-2 data product is the final level, and contains the gravity field as spherical harmonic coefficients. This level also include the GRACE orbits and ancillary data [Case et al., 2010].

4.2   Filtering of the models

The GRACE data is inflicted with correlated errors, that has to be taken into account when doing analyzes. Because of the satellite orbit geometry, a longitudinal striping pattern emerges. The near polar orbit and ranging between the twin satellites, gives a high along track sensitivity [Kusche et al., 2009]. These errors can be taken care of with the use of different filtering techniques, the two methods that will be described in this section is *isotropic filtering*(Gaussian smoothing) and *non isotropic filtering*.
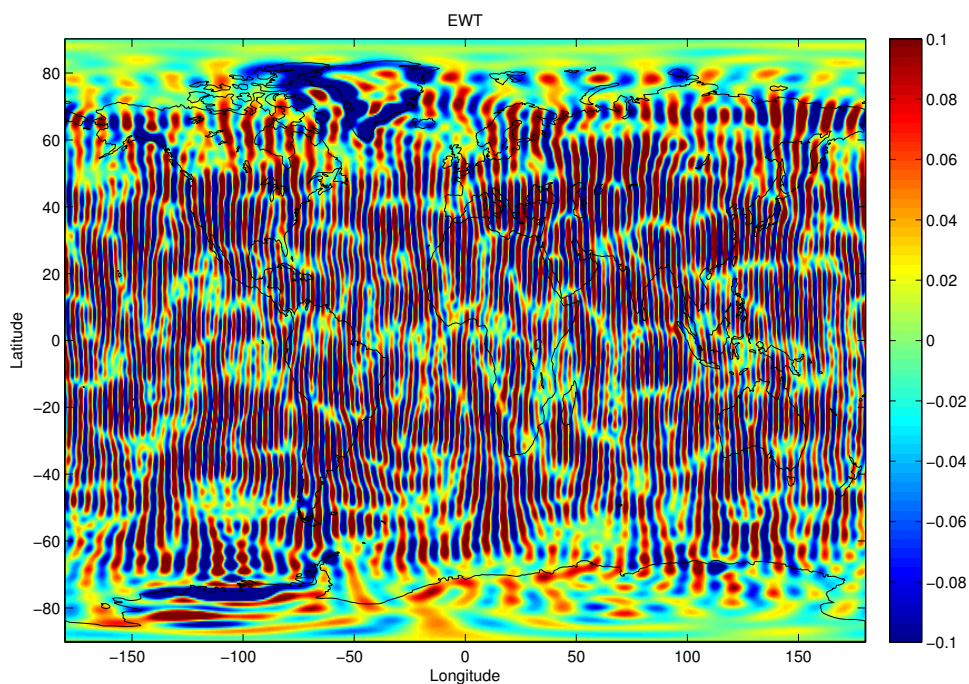

Figure 4.1:   *Non-filtered GRACE solution for Equivalent Water Thickness(EWT)*
[m/yr].

In figure 4.1 the trend from GFZ's GSM model is displayed. All spherical harmonic degrees up to degree and order 90 have been used. The C_{20} has also been replaced with SLR values. With not applying any filter to the model, a distinct longitudinal striping pattern can be seen, and gives little or no information about the gravity field. The striping pattern is most dominant between latitude 60°S and latitude 60°N. This is because of the near-parallel orbits of the satellites at those latitudes.

4.2.1   Gaussian Smoothing

Gaussian smoothing is an isotropic filtering method, all axes are treated equally. Wahr et al.(1998) propose a spatial averaging function for noise reduction of the GRACE-data, a method with a Gaussian shaped kernel. The weighting function, W, is not dependent on the direction, only the distance between the points of computation, and this makes the Gaussian smoothing an isotropic method. $W(\alpha)$ can be calculated with

$$W(\alpha) = \frac{b}{2\pi} \frac{e^{-b(1-\cos\ \alpha)}}{1 - e^{-2b}} \tag{4.1}$$

$$b = \frac{ln(2)}{(1 - \cos(\frac{r}{a})),} \tag{4.2}$$

where r is the averaging radius and α is the angle between the computation points(or distance). Equations 4.1 and 4.2 are normalized averaging functions, to compensate for errors in short wavelength spherical harmonics [Wahr and Molenaar, 1998]. Equation 4.1 is nonzero for all values of α and this will make the signals leak into surrounding areas. This leakage-effect will be described closer and handled in chapter 6 which are explaining the leakage effect of the area of Greenland.

A numerical method for approximating the weighting factors has been proposed by Chambers(2006), and can be calculated by

$$W_n = exp\left[- \frac{(\frac{nr}{2a})^2}{ln(2)} \right] \tag{4.3}$$

where n is the spherical harmonic degree. Equation 4.3 can be used in the spherical harmonic synthesis, and here expressed for surface mass densities (explained in section 2.4):

$$\Delta\bar{\sigma}(\theta, \lambda) = \frac{2\pi a_e \rho_{ave}}{3} \sum_{n=0}^{n_{max}} \frac{2n+1}{1+k_n} W_n \sum_{m=0}^{n} \bar{P}_{nm}(cos\theta)$$

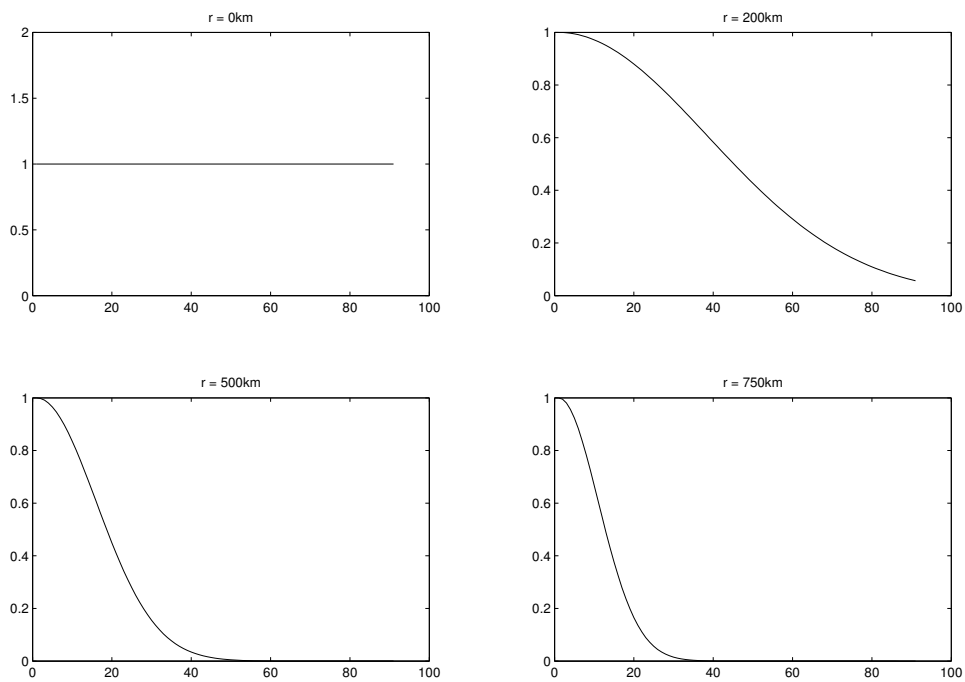$$\cdot (\Delta\bar{C}_{nm}cos\ m\lambda + \Delta\bar{S}_{nm}sin\ m\lambda) \tag{4.4}$$

Figure 4.2: *Gaussian smoothing with kernel radii of 0km, 200km, 500km and 750km.*

Figure 4.2 shows the Gaussian smoothing with different smoothing radii. In order to remove all the correlated errors in the GRACE-data, a large smoothing kernel needs to be applied. This is because of the non-isotropic character of the correlated errors.

The effect of the different smoothing kernels is shown in figure 4.3, on the GSM-model from GFZ. In the upper-left corner no smoothing is applied and the striping is distinct. A 200 km Gaussian radius is shown in the upper-right corner, and there is still some striping pattern to be observed. In the bottom two figures, a radius of 500 km and 750 km has been applied to the model, and the striping pattern is not visible in either of them. It would probably be most accurate to use the 500 km kernel to keep as much information as possible.
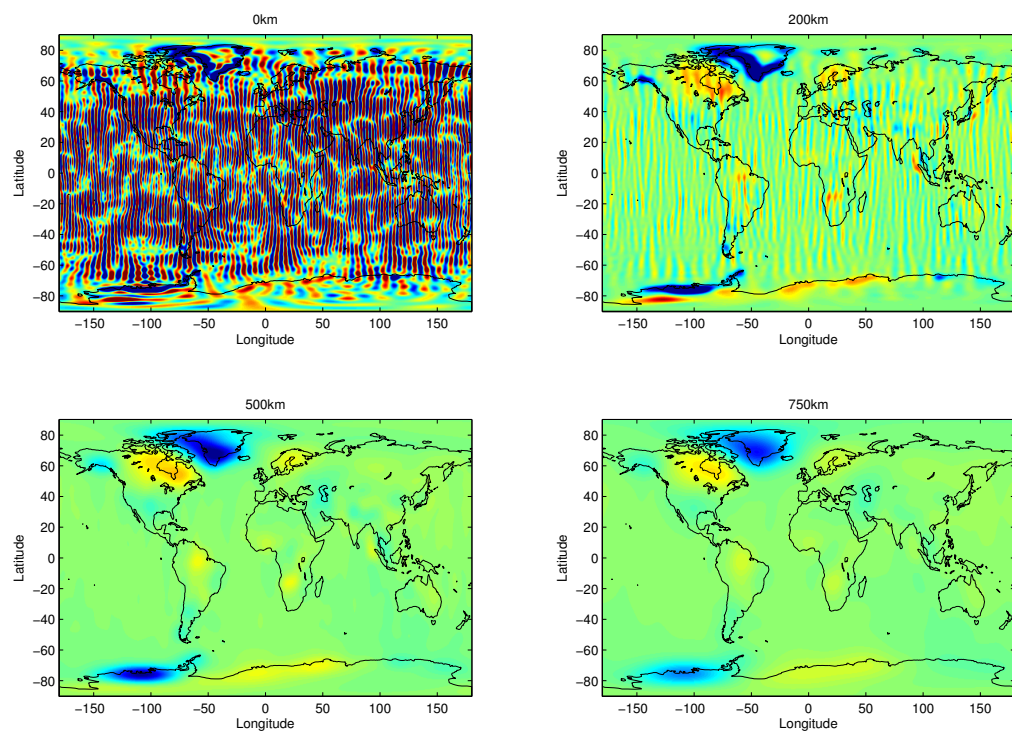
Figure 4.3: *Different filtering radii, represented as EWT for the GSM model [m/yr].*

4.2.2   Non-isotropic smoothing

The standard filtering method has been the Gaussian smoothing, and has been used in GRACE analysis. Kusche et al.(2009) proposes another method for dealing with correlated GRACE errors, which is a *non-isotropic smoothing*. This method has its purpose to decorrelate the GRACE solutions, but keeping the data information provided from GRACE. The filtering method is based on using an a priori

synthetic model of the observation geometry. This results in decorrelated kernels, where the axis system is not symmetric, making it a non-isotropic filter[Kusche et al., 2009].

There are several different non-isotropic filters available, DDK1-DDK8, provided by different processing centers, and are distributed from ICGEM[1]. In this thesis the model of DDK1 will be used, in case of the non-isotropic filtering method, for further analysis. DDK1 corresponds to a Gaussian smoothing radius of 530 km [Kusche et al., 2009]. A Gaussian smoothing of 500 km will be used in the analysis of global gravity fields and in the computations of leakage effects in section 6, for that reason the DDK1-solutions has been chosen in the comparison of models.

4.3 Time Series Analysis of the global gravity field variations

The different processing centers provide monthly GRACE-derived gravity solutions, over several years. This section will investigate the different time series and look at the trend for the different models. The models represented are from GFZ Release 05, AIUB Release 02 and ITSG-GRACE2014, described in section 3.2.

This section will describe the computation of trend, comparison between the Kusche-filtered model and GSM-model with Gaussian filter, and a comparison between the different gravity solutions. All have been done in terms of Equivalent Water Thickness [m/yr].

---

[1]Data can be collected at **http://icgem.gfz-potsdam.de/ICGEM/**

4.3.1   Calculation of trend

The monthly GRACE-solutions makes it possible to calculate the trend for each coefficients over a time period. In equation 4.5 the linear(a)- quadratic(b)-, annual(A)- and semiannual(S)-trend are given.

$$\left.\begin{array}{c} C_{nm}(t) \\ S_{nm}(t) \end{array}\right\} = \left\{\begin{array}{c} C_{nm}(t_0) \\ S_{nm}(t_0) \end{array}\right\} + a\Delta t + \frac{1}{2}b\Delta t^2$$

$$+ A cos[\omega\Delta t + \Phi_A] + S cos[2\omega\Delta t + \Phi_S] \tag{4.5}$$

where ΔT is the time difference($t - t_0$), ω is the period and the Φ terms represent cosine and sine term for annual and semiannual trend.

In further computations only the linear and quadratic term has been estimated by least square adjustment. This is because this thesis has its focus on the long term trend over a time period and not the periodic effects. The quadratic term needs to be calculated to give a correct estimate of the linear trend. This will be investigated further in section 4.3.2.

For further calculations equation 4.6 have been applied, and annual and semiannual term is not considered, since they did not affect the trend calculations.

$$\left.\begin{array}{c} C_{nm}(t) - C_{nm}(t_0) \\ S_{nm}(t) - S_{nm}(t_0) \end{array}\right\} = a(t - t_0) + \frac{1}{2}b(t - t_0)^2 \tag{4.6}$$

The coefficients are weighted with the standard deviations from GRACE-solutions when calculating the trend, and the weighting is given by

$$P_{C_{nm}} = \frac{1}{\sigma^2_{C_{nm}}(t)} \tag{4.7}$$

In equation 4.7 the standard deviation, $\sigma^2_{C_{nm}}$, is presented for the cosine term. The same statement can be for the sine term as well.

The predictions do not give exact values, and the errors need to be estimated. In addition the estimates of the effect on these errors on derived quantities have to be considered. Formal error propagation can be calculated from the standard deviations for the trend to the standard deviation of i.e. geoid height(N) or equivalent water thickness. The trend coefficients are used in the spherical harmonic synthesis, and gives for example EWT [m/yr].

4.3.2   Gravity field trend for the different GRACE-solutions

The different GRACE-solutions can give different results when estimating the grav-
ity field of the Earth. Due to differences in how they calculate the level-2 data
product, the changes in global gravity field can vary. In this section the global
trend of Equivalent Water Thickness has been studied and compared for the dif-
ferent models.

The quadratic term of the trend needs to be calculated in order to get a correct
estimate of the trend. In figure 4.4, the quadratic term has not been calculated
in the least square adjustment, and it is possible to observe that the trend is
actually positive for the areas of Greenland and Antarctica, where it is expected
a downward trend. Where it is expected to observe the GIA effect, Canada and
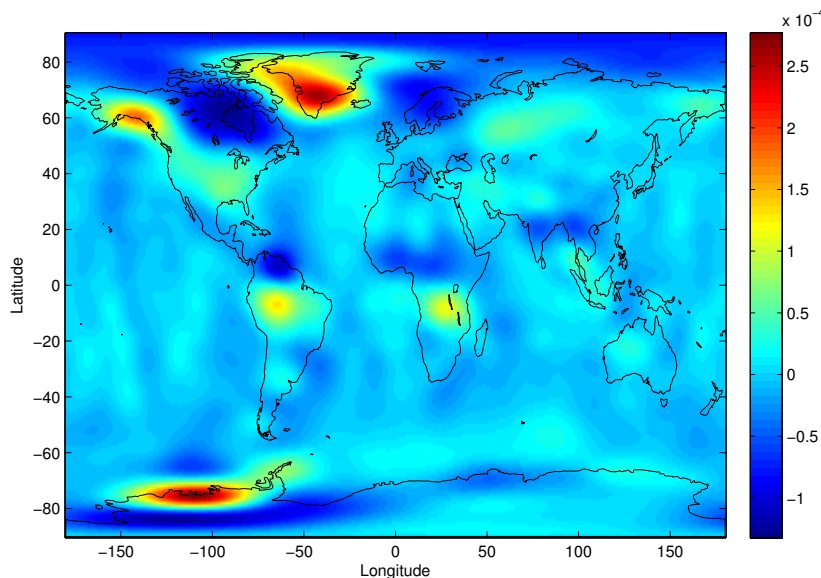Fennoscandia, the trend is negative.

Figure 4.4: *Example of global gravity field(EWT in terms of [m/yr]), without taking
the quadratic term into account. DDK1 solution.*

In figure 4.5 the time series for S_{21} is presented with linear and quadratic trend. As
it is possible to see the linear trend is increasing over the whole period, and a better
estimate is given by the quadratic trend. Until 2009 the trend is clearly increasing,
but after this period a decreasing trend can be observed, and the quadratic term
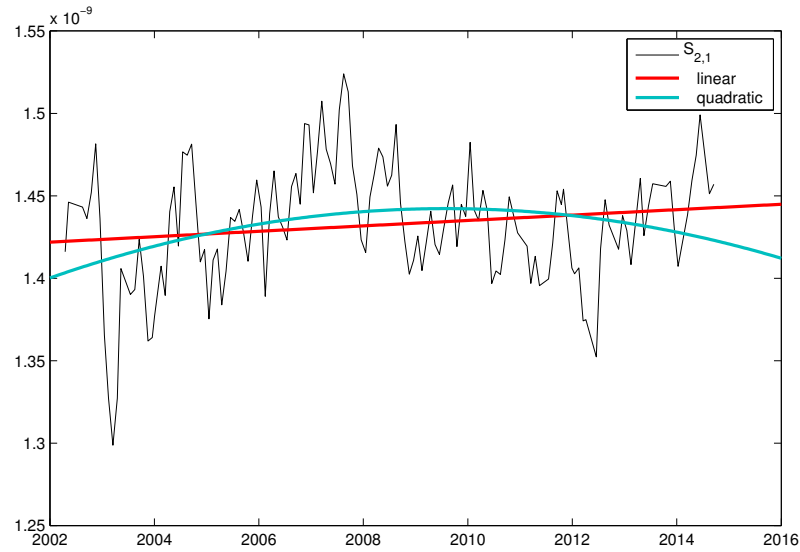are interpreting this.

Figure 4.5: *Time series for S_{21}, showing difference in quadratic and linear trend.*

The trend of the global gravity field spanning from April 2002 to September 2014 from the Kusche-filtered model are shown in figure 4.6. In figure 4.7 the global gravity field for the same period from GSM-solution are shown, with a 500 km Gaussian filter. No Gaussian filter needed to be applied to the Kusche-filter model, because the trend is not correlated with the striping pattern.

The trend in the gravity field are dominated by GIA and ice melting. Over Fennoscandia and the Canadian shield the GIA-effect is visible by the increasing trend, represented as red and orange areas. The cryospheric mass changes can be observed over Greenland, Antarctica, glacier melting can also be observed in Alaska. It shows a decrease in the gravity field, and it is due to the ice melting over the ice caps, and are represented as blue areas in the figures.

It is possible to observe a difference between the Kusche-filtered model(figure 4.6) and the GSM-model with 500 km Gaussian filter(figure 4.7). The Kusche-filtered model is showing a larger variation in the trend, compared to the GSM-model. This implies that maybe a 500 km Gaussian filter is filtering out some of the signal.

Figures 4.8 and 4.9 shows the trend of the solutions from University in Bern(AIUB) and the University in Graz(ITSG), with a 500 km Gaussian smoothing. There are

no huge differences between the two solutions when it comes to calculating the trend, but they both differ from the GFZ solutions. They show a larger trend in EWT compared to GSM-solution, even though the time period are shorter. When compared to the Kusche-filtered model they do not differ that much, but the mass gain over Antarctica, observed in figure 4.6, are not that noticeable in figures 4.8 and 4.9. Again, it can be assumed that some of the signal has been filtered out.
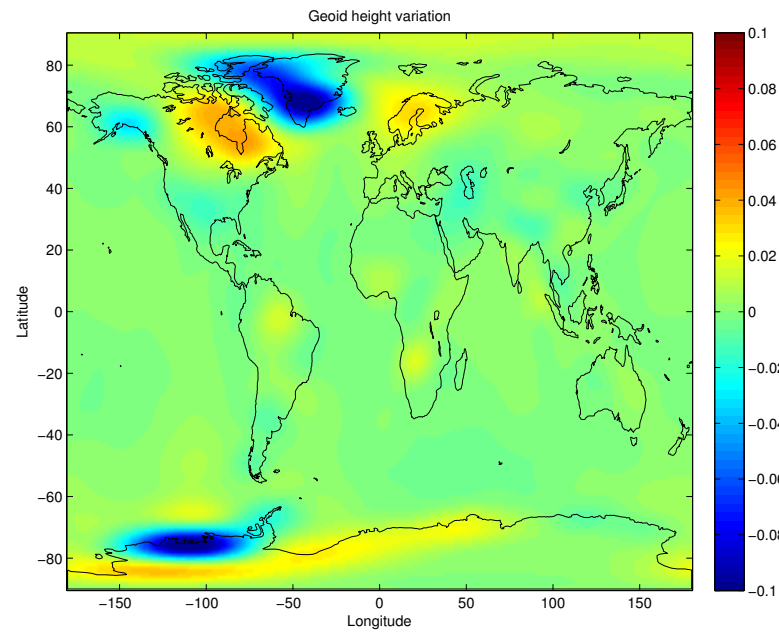
Figure 4.6: *Kusche-filtered model in terms of [m/yr] EWT, DDK1 from GFZ, with quadratic trend estimated.*
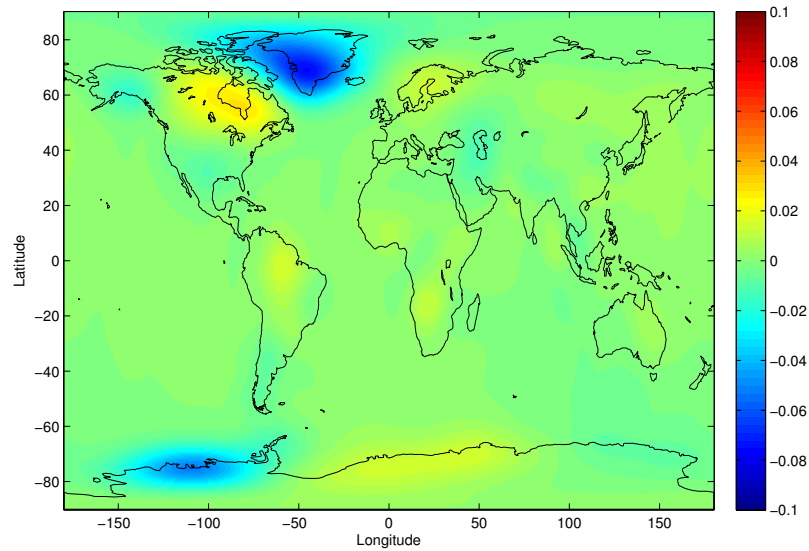

Figure 4.7: *Global model in terms of [m/yr] EWT from GFZ(GSM), smoothing radius 500 km.*
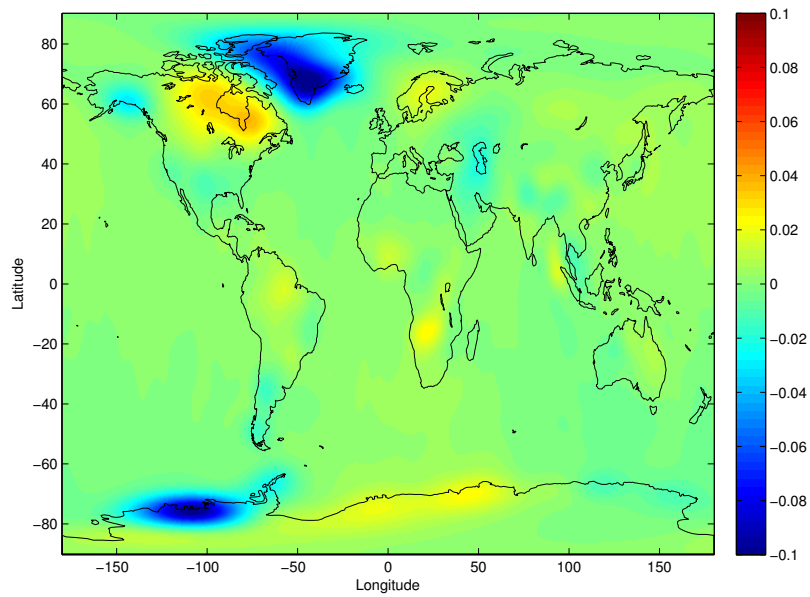
Figure 4.8: *Global model in terms of [m/yr] EWT from AIUB, smoothing radius 500 km.*
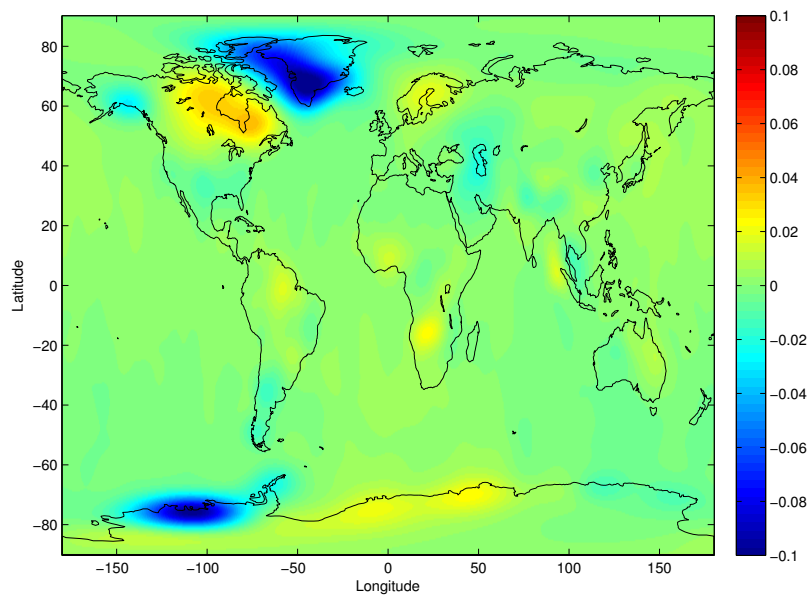

Figure 4.9: *Global model in terms [m/yr] EWT from ITSG, smoothing radius 500 km.*

Chapter 5

Lower degree spherical harmonics

5.1 The Earth's dynamic oblateness

The flattening of the Earth cause a large discrepancy of the Earth's gravitational field from a homogeneous sphere, and the gravitational potential can be expanded into this spherical harmonic series(based on the spherical harmonic series in section 2.3)

$$
V = \frac{GM}{r} \left\{ 1 - \sum_{n=2}^{\infty} \left(\frac{a}{r} \right)^n J_n P_n(cos\theta) \right.
$$
$$
\left. + \sum_{n=2}^{\infty} \sum_{m=1}^{n} \left(\frac{a}{r} \right)^n [C_{nm} cos\ m\lambda + S_{nm} sin\ m\lambda] P_{nm}(cos\theta) \right\} \tag{5.1}
$$

where J_n represents the zonal harmonics and C_{nm} and S_{nm} are the tesseral harmonics. The notation used for zonal harmonics is J_n and it follows from equation 5.1 that $J_n = -C_{n0}$. The satellites are influenced by the J_2-coefficients(and other low degree harmonics) and is therefore used to determine low degree spherical harmonics [Hofmann-Wellenhof and Moritz, 2006].

The C_{20} coefficients, or J_2, describes the Earth's dynamic oblateness and is a function of the difference between equatorial and polar radii of the equipotential surface of the gravity field that best fits the mean sea level [Cheng et al., 2013b].

5.1.1 Different SLR-solutions for lower degree spherical harmonics

There are different providers of SLR-solutions for lower degree spherical harmonics to give a better estimates of these coefficients. In this section the longterm solution from CSR and the solutions from GRACE technical note #7(TN7) and from the University in Bern(AIUB) are compared, and their properties are presented in table 5.1.

Model name	Time Span	Satellites
Long term	1976 – 2011	LAGEOS-1 and 2, Etalon-1 and 2, Starlette, Stella, Ajisai and BEC
TN7	2001 – 2013	LAGEOS-1 and 2, Starlette, Stella and Ajisai
AIUB	2003 – 2014	LAGEOS-1, LAGEOS-2, Starlette, Stella, AJISAI, Beacon-C, LARES, Larets, Blits

Table 5.1: *SLR-solutions from CSR, TN7 and AIUB*

Long term SLR-estimates from CSR

A long term estimate of SLR-values are provided by CSR and is based on up to 8 satellites, LAGEOS-1 and 2, Etalon-1 and 2, Starlette, Stella, Ajisai and BEC [Cheng et al., 2013a].

Since 1979 a decrease in J_2 has been observed, this decrease is mainly because of glacial isostatic adjustment. Cheng et al.(2013) observes that the expected linear trend for J_2 appears more quadratic than linear, and also finds a deceleration in the Earth's oblateness. This observation can come from the changes in rate of the mass redistribution, and is due to climate changes and the melting of ice over land area.

SLR-values from GRACE technical note # 7

Technical note # 7 refers to SLR-estimates from the Center of Space Research(CSR) at the University of Texas in Austin, with monthly estimates for C_{20}. These estimates are based on five geodetic satellites, LAGEOS-1 and 2, Starlette, Stella and Ajisai. They use a background gravity model that is consistent with GRACE Release-05, and includes the same Atmosphere-Ocean and De-aliasing product(AOD). They recommend to replace the C_{20}-values from the GRACE GSM-files of the GRACE release RL05a [Cheng and Ries, 2013].

SLR-values from University in Bern

University in Bern provides monthly estimates of the C_{20}-coefficients from SLR, up to degree and order 10. The AOD-product for Release-05 has been used for de-aliasing, and should be comparable to all GRACE products [Sosnica, 2014].
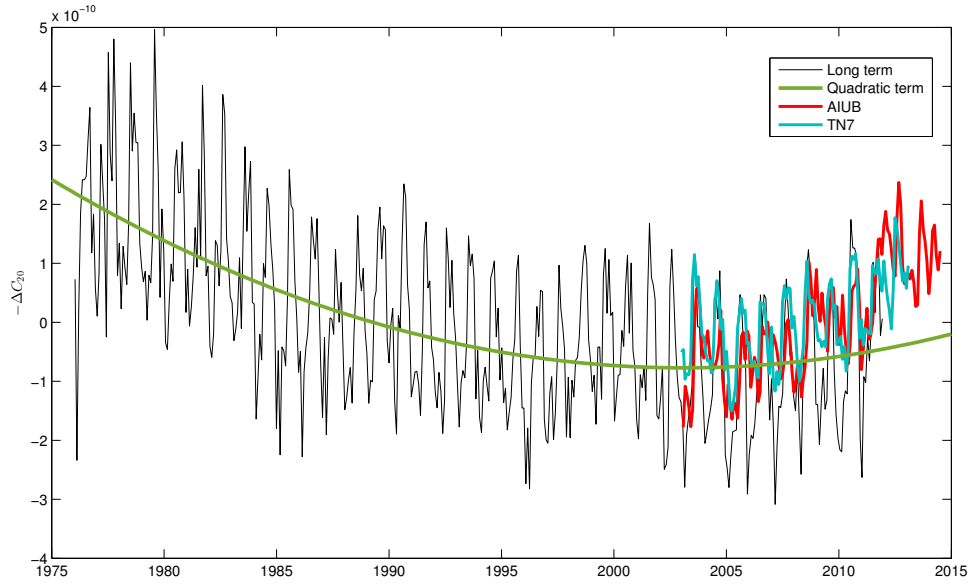
Figure 5.1: *30 days estimates for $-\Delta \bar{C}_{20}$ from SLR. Long term, AIUB and TN7. The quadratic trend for the long term estimate is represented with a green curve.*

The ongoing isostatic adjustment(GIA) from the last ice age and mass exchanges due to climate changes, cause variations in C_{20}. The trend is expected to be linear due to GIA, but Cheng et al.(2013) observes a deceleration in the decreasing rate of J_2 over the last decades. The deceleration in J_2 can be due to the present-day ice melting of the continental glaciers. Figure 5.1 shows 30 days estimates of J_2 from 1976 to 2011(black line) and solutions from AIUB and TN7(red and blue lines). The green curve shows the quadratic trend for the long term SLR-solution. In the long term estimate it is possible to observe a downward trend from 1976 to 1995, and it decelerates from 1995 to 2011 [Cheng et al., 2013a]. The estimates from AIUB and TN7 fits together with the long term estimate, but indicates an increase the last years of observation.

5.2   SLR values for Earth's dynamic oblateness

SLR-data provides a good method for measuring the long term variations of C_{20}. Because GRACE-derived C_{20} variations are affected by tide-like aliases, the SLR-data for these values are of good use [Cheng et al., 2013a]

This section will take a closer look at the SLR-estimates from TN7 and AIUB, compare the SLR-estimates and look at the effect of lower degree spherical harmonics in the spatial domain.
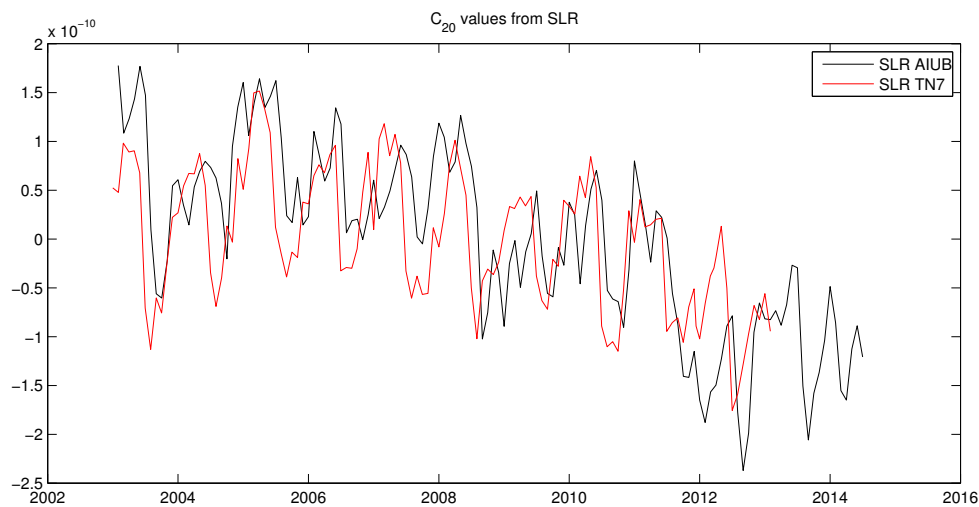
Figure 5.2: $\bar{C}_{20}$ *SLR-values, C_{20}-mean*

The mean deviation, describing the variations around the mean value, are presented for the SLR-values in figure 5.2. The values considered are from GRACE technical note #7 and from the University in Bern. A displacement can be observed between the two SLR-solutions, but they are quite close. The correlation between the two solutions was calculated to 74% for the period January 2003 to December 2012.

There are two main issues concerning the coefficients

1. short term variations where it is possible to observe large correlations between the coefficients.

2. long term variations where the trend coefficients does not differ to a large extent.

The last issue is the one that are most relevant for this thesis.

The trend of the SLR-solutions in figure 5.3 are showing a decrease in the coefficients over 12 and 11 years period. The trend for the AIUB solution is steeper than the trend from Technical note #7. In figures 5.4 and 5.5 the individual trend lines for geoid height are shown in meters, and the decrease in the SLR-coefficients are relatively small, -8.13×10^{-5} m/yr and -1.53×10^{-4} m/yr respectively. The scale of the y-axes are also different, and are showing an offset of about 20 cm between the two solutions. Even though they differ in scale, the relation between the two solution are relatively high, with a correlation of 64%.
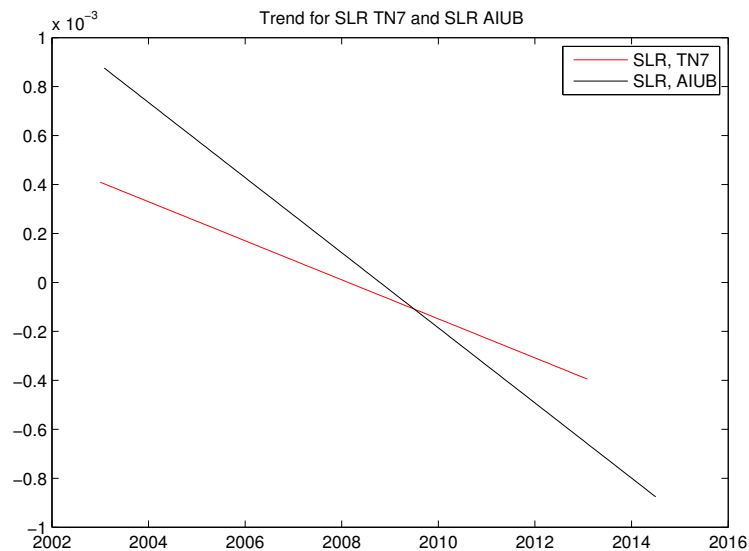

Figure 5.3: *SLR-values from Technical Note 7 and AIUB in terms of geoid height [m], mean deviation.*
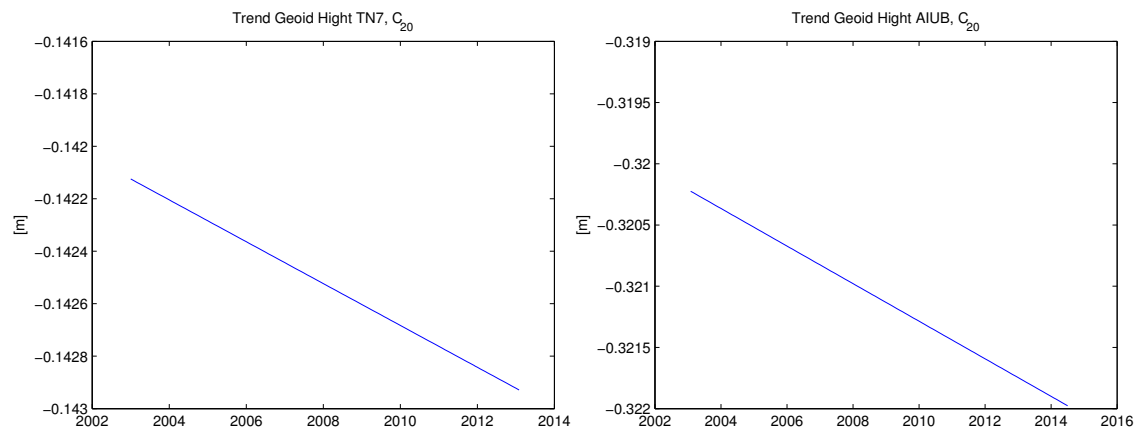
Figure 5.4: *SLR-values from Technical Note 7, trend function for geoid height.*

Figure 5.5: *SLR-values from University in Bern, trend function for geoid height.*

5.2.1   The effect of SLR-values for the C_{20} coefficients

As stated earlier in section 5.1, the C_{20} coefficients describes the flattening of the Earth. Because of the uncertainty in the lower degree spherical harmonics, the signal of the C_{20}-coefficients from GRACE are dominant in the gravity solution. If this is not taken into account, the spherical representation of the gravity field will have this manifested into it, shown as a belt from approximately degree 30 to 90. With the use of SLR-values for these coefficients, this effect will disappear.

In figure 5.6 the SLR values has not yet been replaced for the C_{20} coefficients, and a distinct band is visible in the northern and southern parts of the map. It is still possible to see geophysical signals, but the effect of C_{20} manifest the surrounding areas.

When the C_{20} coefficients from the GRACE-model are replaced with SLR-values, the effect described above is removed, as seen in figure 5.7. This gives a much more accurate estimate for the geoid height(or any other value of interest) and it is easier to interpret without the disturbing signal.
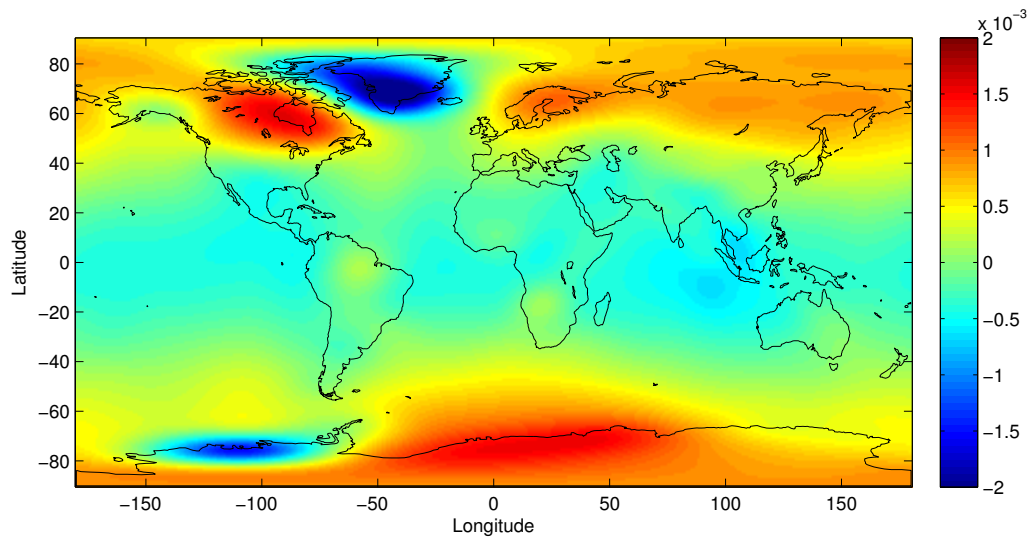
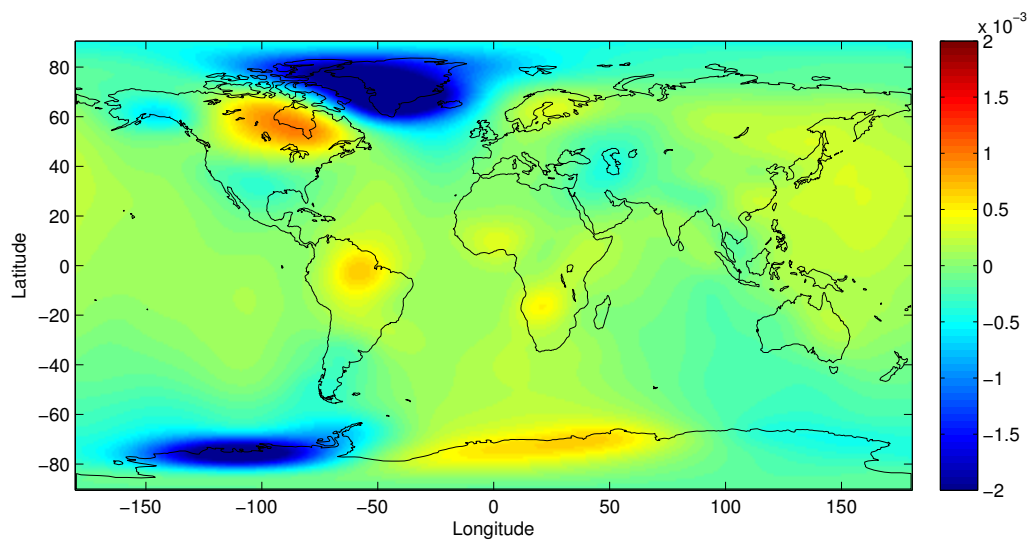**Figure 5.6:** *Geoid height [m/yr], n=0:90 with not adding SLR-values for C_{20}. Model: GFZ-DDK1*

Figure 5.7: *Geoid height [m/yr], n=0:90 when adding SLR-values for C_{20}. Model: GFZ-DDK1*

5.3   Comparison of C_{20} between GRACE and SLR

In this section C_{20}-coefficients from the different models will be compared with the SLR-values from Technical Note 7 and University in Bern. This will make it possible to decide if the coefficient for Earth's dynamic oblateness should be replaced or if it does not affect the computations.

The C_{20}-coefficients from both GFZ-solutions, GSM and Kusche-filtered, are almost identical, and therefore only the GSM-solution has been considered in this section.

Figures 5.8, 5.9 and 5.10 compares the different GRACE-solutions to the SLR-solutions. The C_{20} from GFZ are showing large variations in the coefficients, compared to AIUB and ITSG.
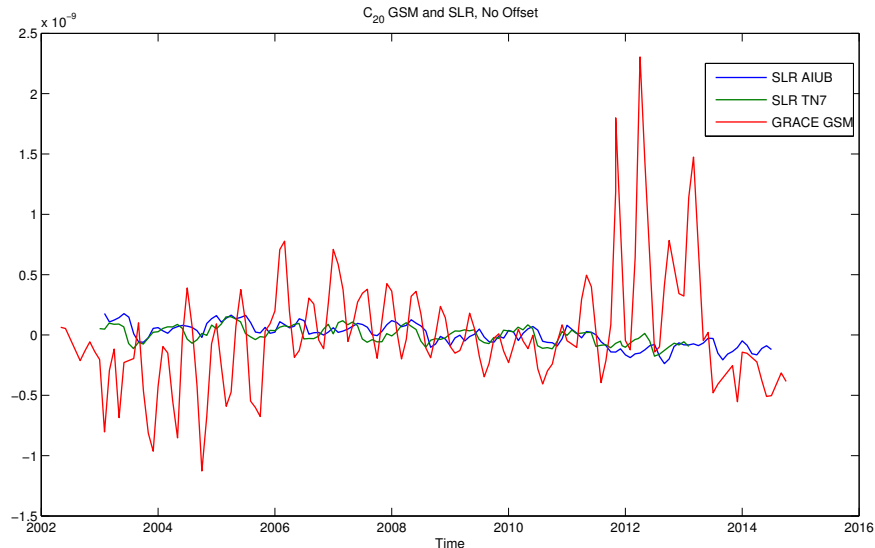
Figure 5.8: *C_{20} values from GSM and SLR (Technical Note 7 and AIUB), C_{20}-mean*

In figure 5.8 there is a clear difference between the SLR-solution and the GRACE-solution from GFZ(GSM), almost no correlation. Also, in the GFZ solution there is one trend from 2002 to 2008, and another trend from 2008 to 2014. There are huge peaks in the beginning and the end of the period. The GRACE-solutions from AIUB and ITSG are better correlated to the SLR-solutions, but there are still some spikes and offsets.
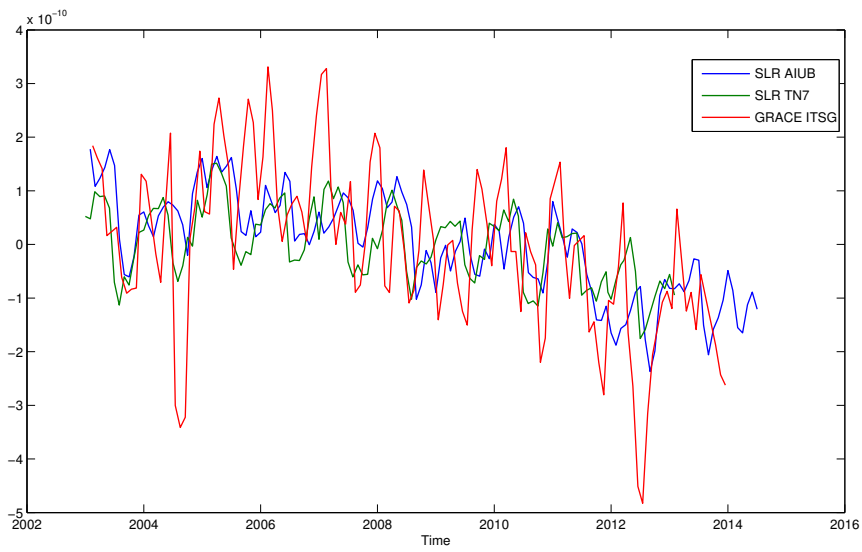
Figure 5.10: *C_{20} values from ITSG and SLR (Technical Note 7 and AIUB), C_{20}-mean*
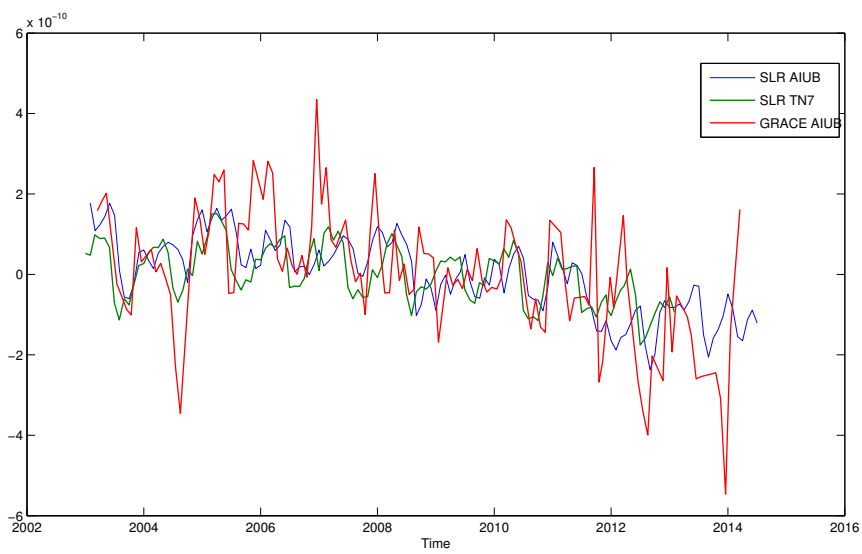
Figure 5.9: *C_{20} values from AIUB and SLR (Technical Note 7 and AIUB),C_{20}-mean*

It should be mentioned that the figures are explaining the variations around the mean value, and that there are offsets between the SLR-solutions and the GRACE-solutions. Table 5.3 shows the correlations and the offsets between the different solution. All values are for the same time period, January 2003 to December 2012. The GSM-solution have large variations in the C_{20}-coefficients, and the correlations in the table are small when comparing to the other solutions. The offsets are also represented in the table, for example an offset between the SLR-solutions is present.

	SLR-TN7	SLR-AIUB	GRACE-AIUB	GRACE-ITSG	GRACE-GSM
SLR-TN7	–	74 % 0.061 m	25% 0.064	57% 0.004 m	19% 0.066 m
SLR-AIUB	74% 0.061 m	–	36% 0.003	56% 0.057 m	31% 0.005 m
GRACE-AIUB	25% 0.064 m	36% 0.003 m	–	49% 0.06 m	11% 0.003 m
GRACE-ITSG	57% 0.004 m	56% 0.057 m	49% 0.060 m	–	25% 0.062 m
GRACE-GSM	19% 0.066 m	31% 0.005 m	11% 0.003 m	25% 0.062 m	–

Table 5.2: *Correlation and offset between the different solutions, where correlation is given in % and offset in geoid hight [m]*

5.4 The effect of the C_{20}-trend

Legendre function, $P_{nm}(cos\theta)$, is a solution of Legendre's differential equation, and is used in the spherical harmonic synthesis. In this section the polynomial of degree 2,

$$P_2(cos\theta) = \frac{3}{4}cos2\theta - \frac{1}{4},$$

has been studied and gives valuable information about the effect of the trend in C_{20}. Since the polynomial can be set as a function of latitude, it can be shown that P_2 changes from pole to pole, but symmetrically over the equator, as seen in figure 5.11.
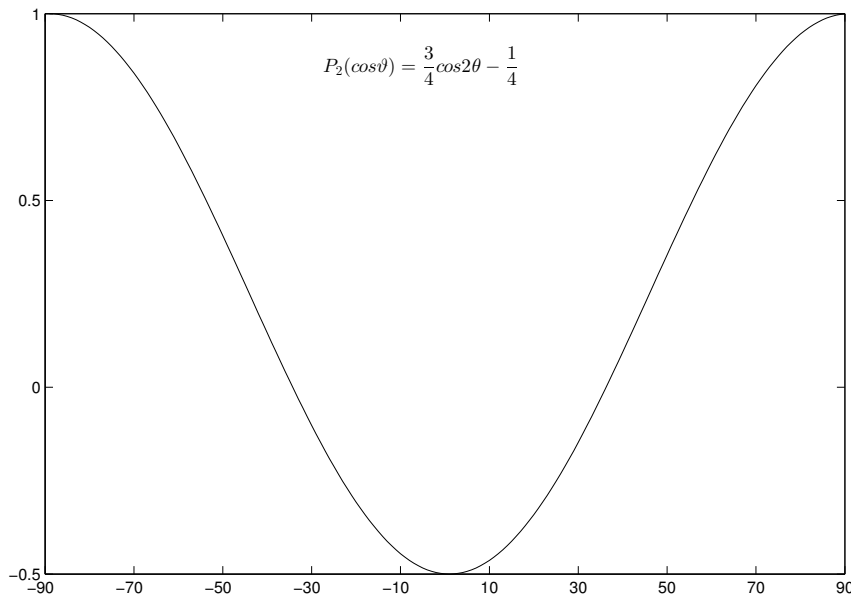
Figure 5.11: P_{20}

The trend of the C_{20}-effect can give an indication on how the C_{20}-coefficients develop in the spatial domain. This gives only information about the spatial structure of the C_{20}-trend. The fully normalized Legendre polynomial is the basis function and are shown in figure 5.11. When only looking at the C_{20}-term the geoid height from equation 2.19 can be simplified to

$$N_{20}(\theta) = R \cdot \bar{C}_{20} \cdot \bar{P}_{20}(\cos \theta) \tag{5.2}$$

For the geoid height represented by the C_{20}-coefficients the values of Legendre polynomials for C_{20} will decrease towards the poles because of the flattening of the Earth, and near the equator the values will increase. In figure 5.12 this effect is visualized for the three different GRACE-solutions. They show the geoid height represented as a the trend in [m/yr].

By comparing the trend of $\bar{C}_{20}$ between the models it is possible to give a conclusion about the significance of the difference between $\bar{C}_{20}$ trend coefficients. In figure 5.13 these comparisons are displayed, with TN7 as basis of comparison. The SLR-solutions gives the best estimates of $\bar{C}_{20}$, and is therefore used as a basis. The figure shows the trend of the $\bar{C}_{20}$ represented as difference in geoid heights(ΔN). For the application of estimating mass changes over a specific region, it is interesting to look at the trend for only this area. In case of this thesis, the Greenland area has been studied, and the yellow fields in figure 5.13 are spanning from 60° to 80° latitude, representing Greenland.

The differences are relatively small, and spans from approximately -70 $\mu m/yr$ to 150 $\mu m/yr$, and there is a close connection to figure 5.12. The comparison between the TN7-solution and the solution from AIUB is the one that have the smallest difference in trend of the area of Greenland, while the three other comparisons differ in a larger scale. A sign change can be observed for the comparison of ITSG and SLR from AIUB, this is because of the larger variations in trend from figure 5.12.

The trends of the C_{20}-coefficients are in fact different, but when computing the trend over a longer time period, the magnitude of the differences are smaller than what is going in to the computations of mass balance over Greenland. This interprets to that it does not matter how the C_{20}-term are processed for the application of estimating mass changes over Greenland(chapter 6).
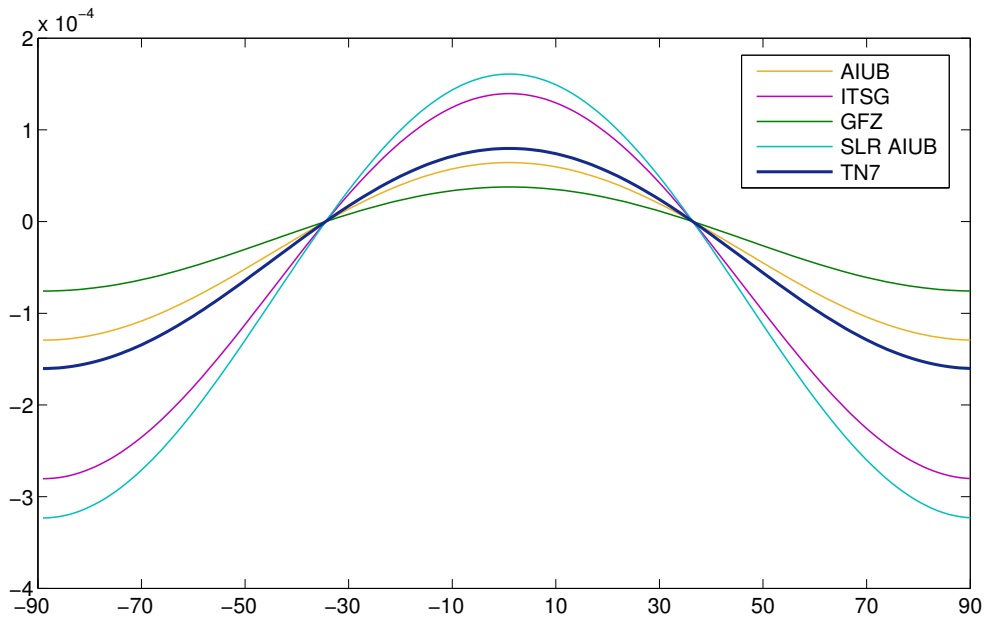
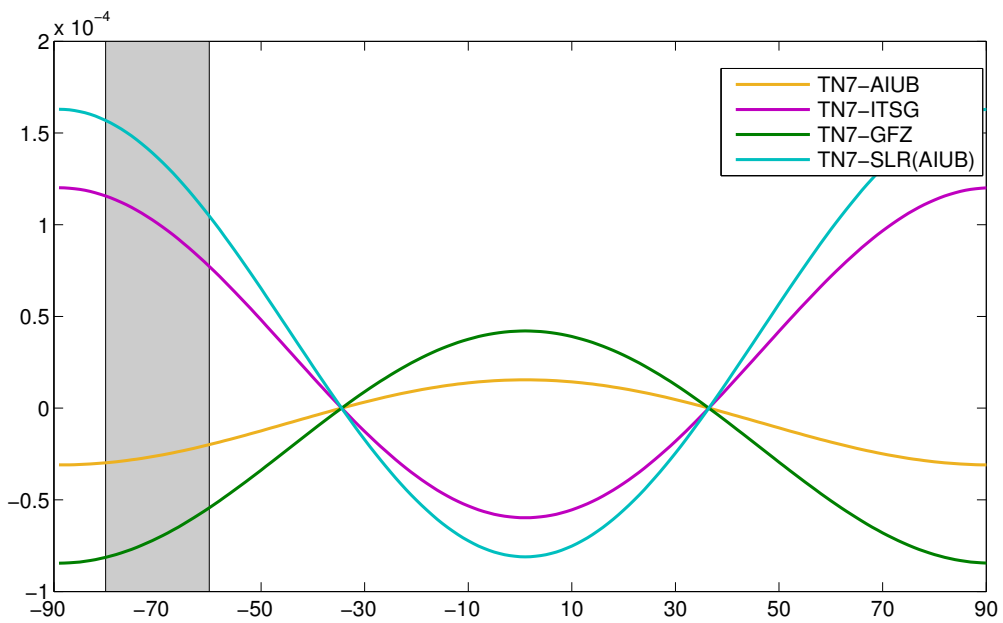**Figure 5.12:** *Individual trends for the different solutions represented as [m/yr]*

Figure 5.13: *Differences in geoid height for the different solutions, with TN7 as basis of comparison. Represented as trend in [m/yr].*

5.5   Correlation

In this section the correlation of the coefficients from GRACE and the coefficients from SLR will be investigated. It is interesting to look at the correlations between different coefficients to be able to determine if more than one coefficient should be replaced. If the correlation between two coefficients are significant, both coefficients should be replaced.

The correlation matrices are obtained from the covariance matrices, and the covariances are scaled with the variance of the two coefficients involved. The correlations are normalized to be in the interval ± 1, and shows how strong the correlations are. The values on the diagonal in a correlation matrix is always 1(100% correlation), and is the correlation between the same coefficient, the matrix is also symmetric above and below the diagonal.

The covariance matrices was given by Krzysztof Sosnica from AIUB. The GRACE variance-covariance(VCM) matrix is from March 2008 and the SLR VCM is from March 2014. In the SLR-solution the geometrical geocenter is set up, but this parameter is pre-eliminated in the final solution. The SLR-solution is constrained with the coefficients of the GRACE-solution, by setting higher degree coefficients to the value of the GRACE-solution. According to K. Sosnica the GRACE VCM's are stable as long as they are based on complete monthly observations, and not affected by orbit resonances.

The covariance in SLR depends on the observation geometry and on the satellites that are used. For example there was only one SLR station in South Africa in 2004, and this station did not provide data for all the months. The only station was established in 2000/2001, and before this period there were no data above this region. The satellite LARES has contributed a lot to the SLR-solutions and was launched in 2012. LARES has decorrelated many parameters because of the different inclination angle, compared to other satellites. This results in different covariance matrices for different months in the SLR solutions(K.Sosnica, private communication).

Figure 5.14 and 5.15 shows the correlation between the coefficients up to degree and order 10. The degree 1 and 0 are not been included in the solutions.
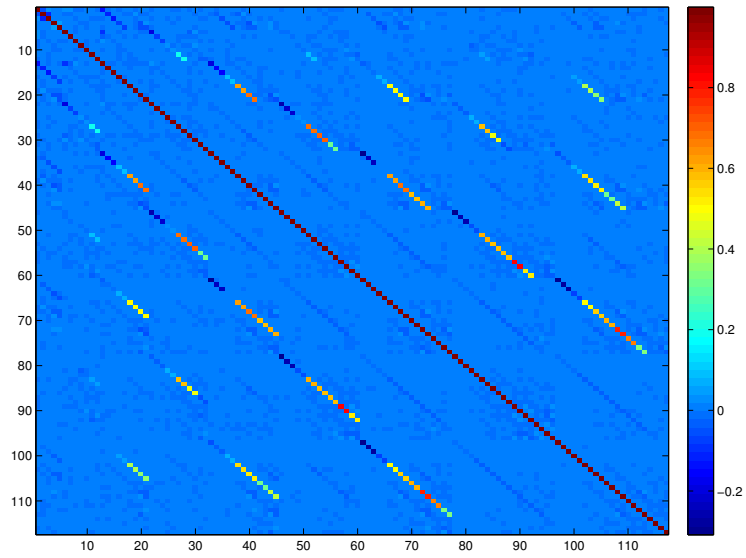
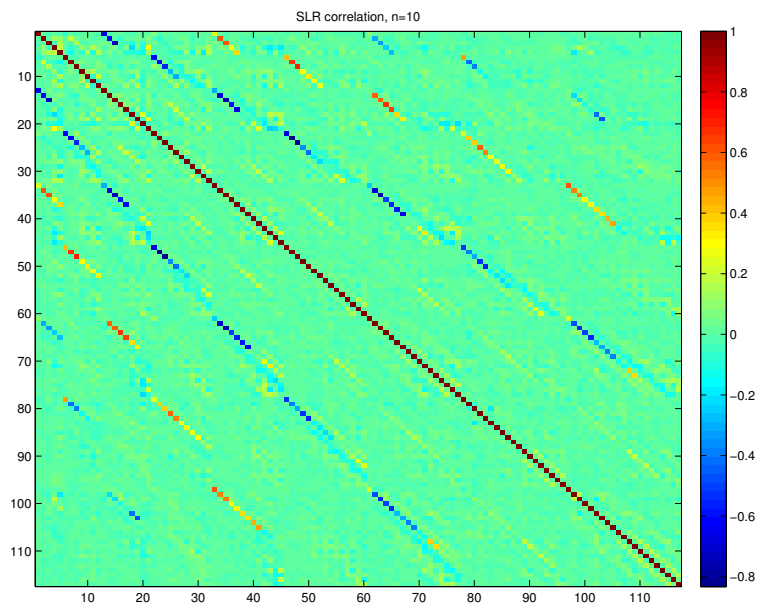**Figure 5.14:** *Correlation between GRACE coefficients up to degree 10*

Figure 5.15: *Correlation between SLR coefficients up to degree 10*

For the purpose of this thesis it is interesting to look at the correlation of C_{20} and other coefficients. The correlations in the lower degree GRACE-data shows little or no correlation between the coefficients, and the maximal correlation for C_{20} and other coefficients up to degree and order 10 is 12.8%. On the other hand, the SLR-values shows larger correlation between the coefficients, and the correlation between C_{20} and C_{40} is 67.5% for march 2008. Because of this correlation one should consider to replace C_{40}-coefficient in addition to C_{20}-coefficient. This has not been done in this thesis, since we only was provided with covariances for one month. Although the GRACE-covariance are stable over time, this is not the case for SLR, and there is not enough basis to know if this correlation is true for all month of the time series.

The correlation matrices in this section are structured by degree and figure 5.16 shows an excerpt of a variance matrix that states how the matrices are ordered and figure that visualize the structure.

PARAM	TYPE	DEGREE N	ORDER M	SIN/COS
1	13	2	0	COS
2	13	2	1	COS
3	13	2	1	SIN
4	13	2	2	COS
5	13	2	2	SIN
6	13	3	0	COS
7	13	3	1	COS
8	13	3	1	SIN
9	13	3	2	COS
10	13	3	2	SIN
11	13	3	3	COS
12	13	3	3	SIN

n,m	2,0	2,1	2,2	3,0	3,1	3,2	3,3	4,0	4,1
2,0	■								
2,1		■							
2,2			■						
3,0				■					
3,1					■				
3,2						■			
3,3							■		
4,0								■	
4,1									■

Figure 5.16: *An excerpt from the covariance file and the structure of the correlation matrices.*

Another way to look at the correlation is to structure the coefficients into blocks dependent on the order m of the spherical harmonic coefficients, starting with order m=0, then m=1, m=2, etc.

Chapter 6

Leakage Effects

Because of the restricted spectral resolution of the gravitational field models and spatial averaging, leakage effects occurs. This means that high frequency signals or errors are mapped into lower frequencies, spectral leakage emerges. In the spatial domain, leakage are displayed as signals spreading. These signals are not concentrated over the area of interest, but are also spreading to the surrounding areas (theoretically over the whole globe).

The leakage effect can be split into two: the *leakage-out* effect and the *leakage-in* effect. The leakage-out explains the signal that emerges to the surrounding areas. As for example, the signal over Greenland is affecting the areas of Fennoscandia, The Canadian Shield and Alaska. But there are also signals leaking out from the surrounding areas that affect the signal on Greenland, these signals are leaking into Greenland, the *leakage-in effect*.

If one wants to calculate the mass change over Greenland (or other areas of interests), this leakage effect has to be taken into account, or one would experience an under- or over estimation of the actual mass change, and in case of Greenland one would experience an underestimation.

6.1   The computation of leakage effect

Baur et al.(2009) are proposing a four-step method for handling the leakage effect. The method is based on the computation of Equivalent Water Thickness(EWT). After doing the spherical harmonic synthesis for EWT over the entire Earth, it is possible to extract the values only containing information over Greenland. This is the first step and gives the initial value(M_1). Because of spatial averaging in the spherical harmonic synthesis, the initial value is not good enough for estimating the mass balance. The second step is to extract initial information over an arbitrary extended area, called M_2. O. Baur(2009) recommends to use isolines for extended areas that does not include other major mass sources. With the initial values it is possible to find the *Intermediate Amplification Factor(IAF)*:

$$IAF = \frac{M_2}{M_1}$$

and from this the mass change can be restored back on to land area in step 3:

$$M_1^* = IAF \cdot M_1$$

With forward gravity modeling, the exact leakage-out effect is provided. This is done by analyzing the gravitational signal obtained from the mass change distribution followed by a synthesis, and this signal is used to calculate the total mass change

$$M_{2,syn}^* = M_2 \left(1 + \left(1 - \frac{M_{2,syn}}{M_2} \right) \right)$$

$M_{2,syn}$ is the forward modeled mass change estimate inside the extended area. $1 - M_{2,syn}/M_2$ express the ratio between the forward modeled mass change estimate and the estimate from step 2, M_2, this gives the amount of signal loss. The *Final Amplification Factor(FAF)* is then calculated by combining the signal loss and the IAF

$$FAF = \frac{M_{2,syn}^*}{M_1}$$

from this the total mass change can be restored back to land area

$$M_{1,syn} = FAF \cdot M_1$$

This is the fourth and last step of the method, and gives the total mass change inside Greenland [O.Baur, 2009].

6.1.1   "Simple Method"

In this section $\Delta\sigma_{in}$ denotes the initial value inside Greenland, $\Delta\sigma_{ext}$ is the value for the extended area and $\Delta\sigma_{in}^*$ is the restored mass change inside Greenland.

Steps 2 and 3 described in previous section can be considered as intermediate steps, and step 4 can be applied directly on to step 1. Baur et al.(2009) recommends to to do all the steps described i section 6.1 because get more realistic mass-change estimates for the forward modeling procedure in the last step. Although it is recommended to do all the steps described, the further calculations in this thesis is based on the "Simple Method", and the computations will be described in this section.

Before starting on the procedure, a spherical harmonic synthesis(SHS) of the GRACE-coefficients is calculated for Equivalent Water Thickness. The synthesis is done for a global 0.5°grid, from n=0:90, and a 500 km Gaussian filter. In the first step, a grid containing only mass change information over Greenland is extracted, all other grid cells outside Greenland is zero. Figure 6.1 displays the initial information over Greenland used in the further calculations. The total mass change for the area of interest is denoted as $\Delta\sigma_{in}$, the initial value.

The next step is the reverse process of the synthesis, the analysis(SHA), to retrieve coefficients representing only local information for Greenland. The calculations for the coefficients are described in section 2.4, but has been carried out as summation of point masses over the whole surface over Greenland, with density computations for each point mass. When doing a spherical harmonic synthesis on these coefficients the total mass change over Greenland, with signal leaking out, is retrieved, and the next step is to rescale the mass change inside Greenland. This is done by the *Amplification Factor(AF)*

$$AF = \frac{\Delta\sigma_{ext}}{\Delta\sigma_{in}},$$

where $\Delta\sigma_{ext}$ is the information over the extended area, and $\Delta\sigma_{in}$ is the initial information over land area. The total mass change can then be restored back on to Greenland

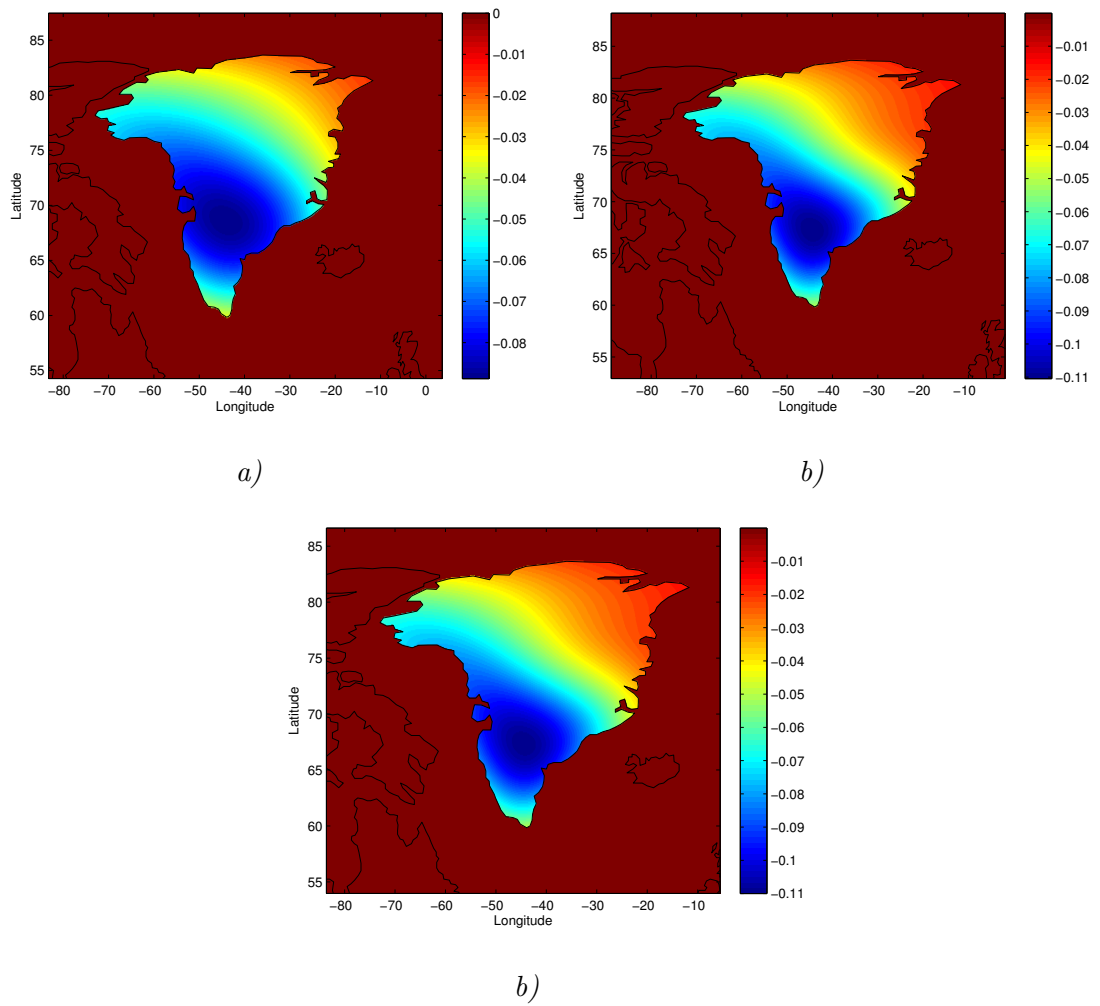$$\Delta\sigma_{in}^* = AF \cdot \Delta\sigma_{in}$$

a)

b)

b)

Figure 6.1: *Initial values containing only information over Greenland, in terms of m/yr EWT. a) GFZ, b) AIUB and c) ITSG*
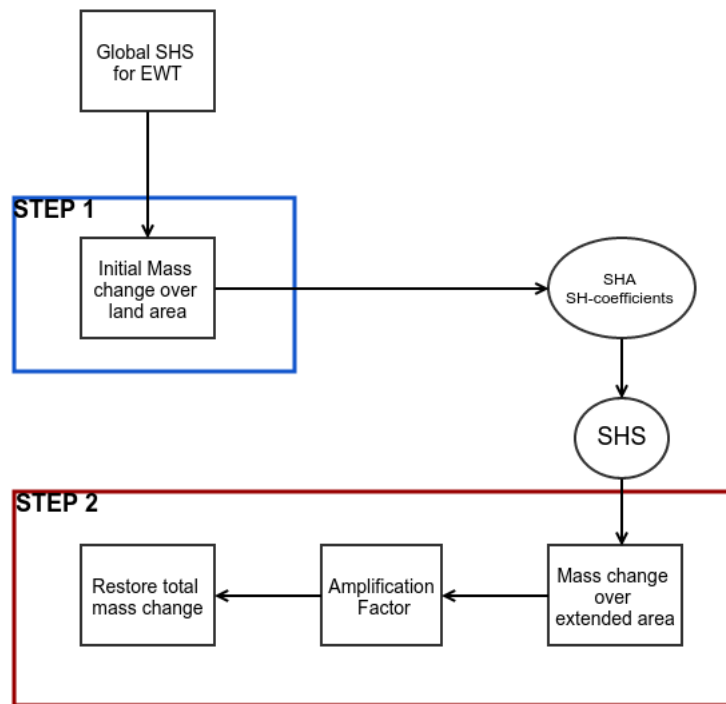
Figure 6.2: *The simple method for estimating mass changes, example of Greenland*

A simple flowchart for the computation of leakage is given in figure 6.2.

The methods described has been used to calculate the leakage-out effect, but can also be done for the calculation of leakage-in effect. The difference is that the individual disturbing sources have to be isolated, and the impact on the region of interest has to be determined. This method is also applicable for any arbitrary area of interest.

6.2   Numerical investigation of the leakage effects over Greenland

In this section the leakage effect for Greenland has been calculated for the different models. In every model a 500 km Gaussian filter has been applied. The Gaussian filter has also been applied to the already Kusche-filtered model, DDK1 from GFZ. This has been done to get a consistent comparison when computing the mass-changes.

In table 6.1 the values of the leakage-out is presented. $\Delta\sigma_{in}$ shows the initial mass information in km^3, and is the value only covering Greenland. The amplification factor (**AF**) is obtained by dividing mass information over extended area with the initial mass information

$$AF = \frac{\Delta\sigma_{ext}}{\Delta\sigma_{in}}$$

The extended area used in the calculations is the northern hemisphere from latitude degree 40 to 90. When multiplying the amplification factor to the initial information, the mass inside Greenland is restored($\Delta\sigma_{in}^*$).

Model	$\Delta\sigma_{in}(km^3)$	**AF**	$\Delta\sigma_{in}^*(km^3)$	$\Delta\sigma_{in}^*$ (km^3/yr)	**Signal loss**(km^3)	No. years
DDK1[1]	-1847.77	1.0451	-1931.11	-167.92	-83.34	11 years and 6 months
GSM	-2001.68	1.0430	-2087.72	-181.54	-86.04	11 years and 6 months
AIUB	-1757.57	1.0428	-1832.76	-183.28	-75.20	10 years
ITSG	-1883.59	1.0429	-1964.38	-182.73	-80.80	10 years and 9 months

Table 6.1: *Values for leakage for the different models. With 500 km radius on Gaussian filtering*

From initial mass information and the final mass change $\Delta\sigma_{in}^*$, the *signal loss* can be calculated, and are represented in table 6.1. The *signal loss* states how much of the signal over Greenland has leaked out to other surrounding areas. In figure 6.3 the effect of the leakage-out is shown. From this figure it can be

---

[1]Kusche filtered

observed that signals from Greenland are leaking out and into Canada, Iceland and Svalbard. And it is this signal that needs to be restored in order to get the real mass information of Greenland.
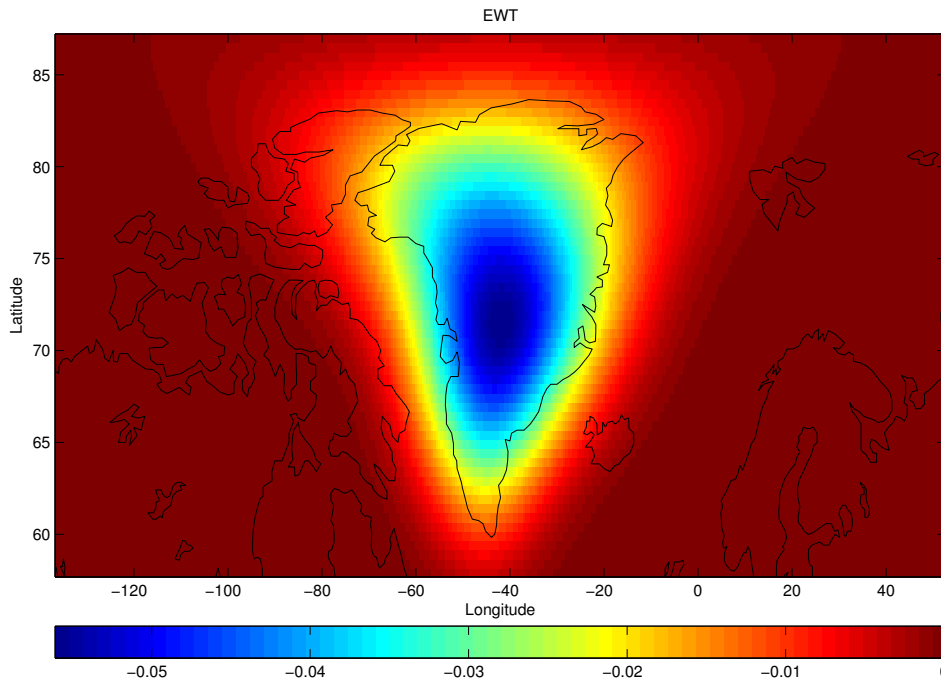

Figure 6.3: *Leakage out from Greenland, expressed in m/yr EWT. GFZ-DDK1*

Because of the different timespan for the models, the mass loss per year is also computed and added to the table. The mass loss per year don't differ much from model to model, but the one that differs from the others, is the Kusche-filtered model from GFZ(DDK1). As stated earlier, DDK1 has already been filtered with a non-isotropic filter from Kusche et al.(2009), and the errors in the GRACE data has already been minimized. A greater mass loss is found using the three other models, this can be a result of errors that has not been filtered out by the Gaussian filter.

Landmass(km^3)	IAF	Signal Loss(km^3)	FAF	Total Change(km^3)
-573.9	1.87	-47.4	1.99	-1143.9

Table 6.2: *Results from O. Baur et al. of volume variations on Greenland. With 500 km smoothing radius. From August 2002 to July 2008.*

In table 6.2 results from O. Baur et al.(2009), for GFZ release-04 with 500 km Gaussian smoothing, are presented, and these results are consistent with the results in tabel 6.1. For the 500 km Gaussian filter on GFZ-model, he observe a signal loss equal to -47.4 km^3 from August 2002 to July 2006. The results in table 6.1 for GFZ, gives a signal loss of -86.04 km^3 for 11.5 years. For a 6 year period(equal to the timespan from O.Baur), this equal to -44.89 km^3. The difference between the two results can come from the different releases, as O. Baur has used release-04 and the calculations done in this thesis is based on release-05. It should also be mentioned that the amplification factor differs from the one in O. Baur's paper, a reason for this is the fact that the computation done in this thesis is based on the "simple method", where step 2 and 3 has been excluded. In addition the Final Amplification Factor calculated by Baur, the leakage in signal is also taken into account and gives an other estimate of the FAF.

Chapter 7

Concluding remarks and outlooks

The goal of this thesis was to compare three different Grace-solutions and estimate a mass loss over a specific area. The solutions was provided by the German Research Center for Geosciences(GFZ), University in Bern(AIUB) and University in Graz(ITSG). Before calculating the mass changes, the global gravity field and the lower degree spherical harmonic was investigated. The focus has been the long term variations, and therefore the trend calculations has been carried out in this thesis. This chapter will summarize and give the final conclusions.

Because of long term variations in the individual coefficients, the quadratic trend needs to be taken into account in the least square adjustment of the spherical harmonic coefficients, to get a reliable estimate of the linear trend. When this trend is taken into the spatial domain through spherical harmonic synthesis, the trend over a time series shows the effect of post glacial rebound in Canada and Fennoscandia, and ice melting over Greenland and Alaska. In addition, mass redistribution is observed in Antarctica. No huge differences between the three GRACE-solutions was observed, but the GSM-model with 500 km Gaussian filter shows a weaker signal all over the globe compared to the other models. The DDK1-solution also shows stronger signals over Canada, Fennoscandia and Antarctica. Because of Gaussian smoothing for the three other solutions, some of the signals has been damped compared to the Kusche-filtered model, and are not giving all the information.

In the comparison between the SLR-solutions, the long term estimate of J_2 shows deceleration in the Earth's oblateness and a quadratic trend is a better fit than a linear trend, while the two other SLR-solutions(AIUB and TN7) shows an increase

from around 2009. Further, the two SLR-solutions from AIUB and TN7 has been compared and they do not differ to a large extent. The correlation between the two solutions are 74%, and the choice of solution in further calculations is not significant. Because of the uncertainty in the lower degree spherical harmonic from GRACE, the signal of the C_{20}-coefficients are dominant in the gravity solution, and needs to be replaced with coefficients from SLR.

When comparing the C_{20} GRACE-coefficients from the three solutions with SLR-solutions, there is a clear variation in the coefficients from GRACE. The GSM-solution is the one with least accuracy and has correlation of 19% to TN7 and 31% to AIUB. The solutions from ITSG is the one with the highest correlation, 57% and 56%. The GRACE-solution from AIUB has a correlation with SLR of 25% and 36%.

The effect of the C_{20}-trend coefficients has been investigated and differences between the solutions has been carried out with the SLR-values from Technical Note 7 as a basis of comparison. The differences are small and spanning from approximately -70μm/yr – 150μm/yr. The magnitude of the differences are smaller than what is going into the computations of mass balance over Greenland, and it does not matter how the C_{20}-coefficients are processed for the application of this thesis.

Covariance matrices for the lower degree spherical harmonics up to degree and order 10 was provided and correlations was carried out. No huge correlations was found in the lower degree GRACE-coefficients, the largest correlation was of 12.8%. However, a much larger correlation was observed from SLR, with highest correlation between C_{20} and C_{40} at 67.5%. From this it should be considered to replace both the C_{20}-coefficient and C_{40}-coefficient from SLR in the GRACE-solution. This has not been done in this thesis, since we only was provided with covariances for one month. Although the GRACE-covariance are stable over time, this is not the case for SLR, and there is not enough basis to know if this correlation is true for all month of the time series. For further investigation, one should consider to look at all the SLR correlations of a time series to get a more reliable conclusion of how to employ the SLR-values.

The leakage effect and the mass balance over Greenland in chapter 6 finds a mass change estimate for the solutions, DDK1, GSM, AIUB and ITSG. For the DDK1-solution mass loss of -1931.11 km^3 has been found, -2087.72 km^3 for GSM, -1832.76 km^3 for AIUB and -1964.38 km^3 for ITSG. The signal loss was estimated to be -83.34 km^3 for DDK1, -86.04 km^3 for GSM, -75.20 km^3 for AIUB and -80.80 km^3 for ITSG. All the estimates has been compared to O. Baur et al.(2009)

and they are consistent. The leakage-in effect has not been taken into account, and further investigations should consider this effect as well, to get an even better estimate. In addition, one should also consider to use all four steps described in O. Baur et al.(2009).

GRACE has provided gravity field data since 2002, and a follow-on mission is due to launch in 2017. GRACE-FO will continue to give global gravity field models, and dedicated gravity satellite missions are of huge interest in the future.

Bibliography

[Barthelmes, 2009] Barthelmes, F. (2009). Definition of functionals of the geopotential and their calculation from spherical harmonic models. *GFZ, Deutsches GeoForschungsZentrum*.

[Case et al., 2010] Case, K. et al. (2010). Grace level 1b data product user handbook. Technical report, Jet Propulsion Laboratory.

[Chen et al., 2013] Chen, J. L. et al. (2013). Rapid ice melting drives earth's pole to the east. *Geophysical Research Letters*.

[Cheng et al., 2013a] Cheng, M. et al. (2013a). Deceleration in earth's oblateness. *Journal of Geophysical Research*.

[Cheng and Ries, 2013] Cheng, M. and Ries, J. (2013). Grace technical note 07, center for space research. `http://isdc.gfz-potsdam.de/index.php?name=News&file=article&sid=131&theme=Printer`. Accessed: 2015-03-04.

[Cheng et al., 2013b] Cheng, M., Tapley, B. D., and Ries, J. C. (2013b). Spherical harmonic coefficients of degree 2. `http://grace.jpl.nasa.gov/data/J2/`. Accessed: 2015-01-02.

[Dahle et al., 2012] Dahle, C., Flechtner, F., Gruber, C., König, D., König, R., Michalak, G., and Neumayer, K.-H. (2012). Gfz grace level-2 processing standards document for level-2 product release 0005. Technical report, Potsdam. (Scientific Technical Report STR12/02 – Data, Revised Edition, January 2013).

[GFZ, 2014] GFZ (2014). The champ satellite. `http://www.gfz-potsdam.de/en/section/earths-magnetic-field/infrastructure/champ/satellite-systems/`. Accessed: 2015-04-29.

[GFZ, 2015] GFZ (2015). Gravity recovery and climate experiment-follow-on (grace-fo) mission. `http://www.gfz-potsdam.de/en/section/globalgeomonitoringandgravityfield/topics/development-operation-and-analysis-of-gravity-field-satellite-missions/grace-fo/`. Accessed: 2015-04-29.

[Hofmann-Wellenhof and Moritz, 2006] Hofmann-Wellenhof, B. and Moritz, H. (2006). *Physical geodesy*. Springer.

[Kusche et al., 2009] Kusche, J. et al. (2009). Decorrelated grace time-variable gravity solutions by gfz, and their validation using a hydrological model. *Journal of Geophysical Research*.

[Mayer-Gürr et al., 2014] Mayer-Gürr, T. et al. (2014). Itsg-grace2014. `http://portal.tugraz.at/portal/page/portal/TU_Graz/Einrichtungen/Institute/Homepages/i5210/research/ITSG-Grace2014`. Accessed: 2015-03-02.

[NASA, 2015] NASA (2015). `http://grace.jpl.nasa.gov/`. Accessed: 2015-04-18.

[O.Baur, 2009] O.Baur, M. kuhn, W. F. (2009). Grace-derived ice-mass variation over greenland by accounting for leakage effects. *Journal of Geophysical Research*.

[Petrov and Boy, 2004] Petrov, L. and Boy, J. (2004). Atmospheric pressure loading service. `http://gemini.gsfc.nasa.gov/aplo`. Accessed: 2015-05-01.

[Seeber, 2003] Seeber, G. (2003). *Satellite Geodesy*. Walter de Gruyter.

[Sosnica, 2014] Sosnica, K. (2014). Contribution of starlette, stella and ajisai to the slr-derived global reference frame. *Journal of Geodesy*.

[Subirana et al., 2011] Subirana, J. S. et al. (2011). Ocean loading. `http://www.navipedia.net/index.php/Ocean_loading`. Accessed: 2015-05-01.

[Torge and Müller, 2012] Torge, W. and Müller, J. (2012). *Geodesy*. Walter de Gruyter.

[U. Meyer, 2011] U. Meyer, A. Jaeggi, G. B. (2011). Aiub-grace03s. `http:`

//www.aiub.unibe.ch/content/research/satellite_geodesy/gnss___
research/global_gravity_field_determination_grace/index_eng.html.
Accessed: 2015-03-02.

[Wahr and Molenaar, 1998] Wahr, J. and Molenaar, M. (1998). Time-variable
gravity recovery from grace. *Journal of Geophysical Research.*